



Room 14-0551
77 Massachusetts Avenue
Cambridge, MA 02139
Ph: 617.253.5668 Fax: 617.253.1690
Email: docs@mit.edu
<http://libraries.mit.edu/docs>

DISCLAIMER OF QUALITY

Due to the condition of the original material, there are unavoidable flaws in this reproduction. We have made every effort possible to provide you with the best copy available. If you are dissatisfied with this product and find it unusable, please contact Document Services as soon as possible.

Thank you.

Some pages in the original document contain pictures, graphics, or text that is illegible.

The Stability of Respiratory Control in Man:
Mathematical and Experimental Analyses

by

David William Carley

B.S.E.E. State University of N. Y. at Stony Brook
(1978)

S.M. Massachusetts Institute of Technology
(1982)

Submitted to the Harvard-MIT Division of
Health Sciences and Technology
in Partial Fulfillment of the
Requirements of the
Degree of

DOCTOR OF PHILOSOPHY

at the

MASSACHUSETTS INSTITUTE OF TECHNOLOGY

June 1985

© David W. Carley 1985

The author hereby grants to M.I.T. permission to reproduce and to
distribute copies of this thesis document in whole or in part.

Signature of Author: _____
Harvard-MIT Division of Health Sciences
and Technology 19 April 1985

Certified by: _____
Daniel C. Shannon
Thesis Supervisor

Accepted by: _____
Ernest G. Cravalho
Chairman, Division Committee on Graduate Theses



The Stability of Respiratory Control in Man:

Mathematical and Experimental Analyses

by

David W. Carley

Submitted to the Harvard-MIT Division of Health Sciences
and Technology on April 19, 1985 in partial fulfillment
of the requirements for the Degree of
Doctor of Philosophy in Medical Engineering

ABSTRACT

Several nonlinear simulation models have been formulated in an attempt to account for the dynamics of respiratory control, including the etiology of Cheyne-Stokes respiration (CSR). Direct experimental validation of these models has not been performed. Our studies show that in conscious man, the power of the ventilatory transient response (TR) is indeed a continuous function of the control system loop gain (LG). We have demonstrated that CSR may be induced by increasing the loop gain, and can represent an enhancement of the non-sustained oscillations seen in normal resting breathing. A minimal linear control system model is described which accurately predicts TR as a function of LG. Using this model, we have demonstrated that LG is determined by the interaction of 2 dimensionless parameters that each combine several physiologic variables. By evaluating these dimensionless parameters the relative stability of any equilibrium point may be readily determined. These findings indicate that mathematical models of respiration can provide an important tool for determining the etiology of clinically important phenomena such as periodic breathing in adults or neonates.

Thesis Supervisor: Dr. Daniel C. Shannon

Title: Associate Professor of Pediatrics
Harvard-MIT Division of Health Sciences and Technology

Name: David W. Carley

Address: 6 Franklin St., Braintree, Ma. 02184

Date of Birth: January 18, 1956

Place of Birth: Endicott, New York

Education:

1978 BSEE	Stony Brook University
1982 SM	Massachusetts Institute of Technology (Elec. Eng.)
1985 Ph.D.	Massachusetts Institute of Technology (Medical Eng.)

Awards and Honors:

1974-1978	N. Y. State Regents Scholarship
1976	Tau Beta Pi
1977-1978	Secretary, N.Y. Omicron Chapter, Tau Beta Pi
1978	Stony Brook Scholar Athlete Award
1978	BSEE - Summa Cum Laude
1978-1979	HST Graduate Fellowship
1979-1982	Surdna Foundation Fellowship

Professional Societies:

1976 -	Institute of Electrical and Electronic Engineers
1978 -	Professional Engineer: Engineer in Training

Major Research Interests:

- 1). Biological Signal Processing
- 2). Mathematical Control Systems Modeling
- 3). Biological Control of Respiration in Health and Disease

Teaching Experience:

1982	Taught Medical School Recitations in Quantitative Physiology
1982	Taught Medical School Recitations in Respiratory Pathophysiology
1983 -	Organized and Teach Seminar Series in Statistical Data Analysis Pediatric Pulmonary Unit, Mass. General Hospital
1984 -	Organized and Teach Seminar Series in Medical Instrumentation Pediatric Pulmonary Unit, Mass. General Hospital

Original Reports

Carley D, Shannon DC. Control Systems Analysis of Respiratory Regulation. In: Proceedings of the International Symposium on "Oscillations in Physiologic Systems: Dynamics and Control". Oxford, U.K.: Institute of Measurement and Control, 1984: 43-47.

Shannon DC, Carley D. Systems Analysis Applied to Studies of Respiratory Control. In: Proceedings of the International Symposium, "Neurogenesis of Central Respiratory Rhythm". Bando1, France: MTP Ltd, 1984.

Carley D, Shannon DC. A Minimal Control System Model of Periodic Breathing. In: Proceedings of the "11th Northeast Bioengineering Conference". Worcester, Ma.: IEEE, In Press.

ACKNOWLEDGEMENT

This single leaf is the most difficult compositional challenge posed for me by the entire manuscript, and truly I feel inadequate to the task. To commit to paper a litany of the enrichment and benefit I have received from so many individuals is virtually to do an injustice to them all. I hope you all know who you are, and forgive, for I yet feel compelled to make the attempt.

For his trenchant advice, support, and encouragement, I owe an immense debt of gratitude to my thesis supervisor, Dan Shannon. By providing a rich and stimulating environment and above all by allowing me the necessary intellectual freedom, he has helped me to develop new perspectives on the nature of scientific research.

Dr.'s Edwin Trautman, Richard Cohen, and Jose Venegas each made substantial and valuable contributions to this work. As members of my advisory committee each filled at one time or another the essential roles of Devil's advocate, Dutch Uncle, and good friend. I am especially appreciative of Jose's assistance in the preparation of my defense.

I must also acknowledge the understanding tolerance, and support of Karen Sullivan and Kaaren Sailer. Their willingness to help, and frequent valuable suggestions are greatly appreciated. The dedication and persistence of Clara Balkas when the chips were down, were an inspiration to me.

Finally, this page would simply be incomplete without a warm word of thanks for the monumental efforts and academic courage of everyone involved in the formation and administration of the Medical Engineering and Medical Physics program. Its curriculum is new and bold, and presented me with a absolutely unique educational opportunity. I am grateful to have been a member of the program's first entering class. The camaraderie and sheer intellectual excitement I have always felt around my classmates have helped me through many dark moments in the last seven years. Thank you all.

DEDICATION

To my parents,

BETSEY AND BILL

for providing a rich environment to grow in
and unwavering support for my education

and to my wife

LINDA

for providing the extra dimension of support
which made finishing worth all the efforts

TABLE OF CONTENTS

ABSTRACT	2
BIOGRAPHICAL SKETCH	3
ACKNOWLEDGEMENTS	4
DEDICATION	5
NOMENCLATURE	8
1. INTRODUCTION	9
1.1 Cheyne-Stokes Respiration	9
1.2 Etiology of Cheyne-Stokes Respiration	10
1.3 Basic Operation of the Respiratory Control System	11
1.4 Stability Criteria	14
1.5 Models of CSR: The State of the Art	15
1.6 Statement of the Problem	18
1.7 The Minimal Modeling Approach	18
1.8 Validation of the Minimal Model	19
2. A MINIMAL MODEL OF HUMAN RESPIRATORY CONTROL	24
2.1 Introduction	24
2.2 The Minimal Model	25
2.2.1 The Controlled System	26
2.2.2 The Controller	30
2.2.3 The Pure Delay	32
2.3 Loop Gain of the Minimal Model	33
2.4 Stability of the Minimal Model	34
2.5 Relative vs. Loop Gain	35
2.6 Defining the Measure of Relative Stability	38
3. VENTILATORY RESPONSES TO TRANSIENT PERTURBATIONS OF ALVEOLAR CO ₂ DURING GRADED HYPOXIA IN MAN	49
3.1 Introduction	49
3.2 Methods	51
3.2.1 Apparatus	51
3.2.2 Experimental Methods	52
3.2.3 Analysis Procedures	55
3.3 Results	60
3.4 Discussion	65
3.5 Conclusions	74
3.5.1 Significance of Results	75
3.5.2 Suggestions for Future Work	76
APPENDIX 1	
Computation of Power Density Spectra	98
APPENDIX 2	
Comparison of Minimal Model to Previous Work	102

APPENDIX 3	
Describing Function Analysis and the Minimal Model	119
REFERENCES	127

NOMENCLATURE

Variable	Description	Units
t	time	s
$\dot{}$	partial derivative	
Q _C	cardiac output	l s ⁻¹
C _{CO₂}	CO ₂ concentration	
C _{vCO₂} (t)	mixed venous CO ₂ concentration	
C _{aCO₂} (t)	mixed arterial CO ₂ concentration	
F _{ACO₂} (t)	alveolar CO ₂ mole fraction	
F _{ICO₂} (t)	inspired gas CO ₂ mole fraction	
P _{CO₂}	partial pressure of CO ₂	torr
P _{vCO₂} (t)	mixed venous CO ₂ partial pressure	torr
P _{aCO₂} (t)	mixed arterial CO ₂ partial pressure	torr
P _{ACO₂} (t)	alveolar CO ₂ partial pressure	torr
P _{ICO₂} (t)	inspired gas CO ₂ partial pressure	torr
P _{CR} (t)	P _{CO₂} (t) at chemoreceptor	torr
P _{aCO₂} ^o	equilibrium value of P _{aCO₂} (t)	torr
P ^B	barometric pressure	torr
P ^W	water vapor pressure at body temp.	torr
K _{s1}	incremental solubility of CO ₂ in blood	torr ⁻¹
K _{s2}	CO ₂ solubility constant	
V _{.ACO₂} (t)	alveolar volume of CO ₂	l
V _{.A}	continuous alveolar ventilation	l s ⁻¹
V _A ^o	equilibrium value of V _A	l s ⁻¹
T ₀	time constant of alveolar equilibration	s
f	frequency	s ⁻¹
f _c	critical (crossover) frequency	s ⁻¹
f _d	disturbance frequency	s ⁻¹
f ₀	corner frequency	s ⁻¹
A(f)	controller transfer function	
A	magnitude of A(f)	l s ⁻¹ torr ⁻¹
B(f)	controlled system transfer function	
B(f)	magnitude of B(f)	torr l ⁻¹ s ⁻¹
B	equilibrium value of B(f)	torr l ⁻¹ s ⁻¹
<A(f)	phase shift of controller	degrees
<B(f)	phase shift of controlled system	degrees
<T _c (f)	phase shift of circulation delay	degrees
LG(f)	loop gain magnitude at f	
<LG(f)	loop phase shift at f	degrees
S	controller setpoint	torr
T _C	pure delay	s

CHAPTER 1

INTRODUCTION

1.

Two facts regarding human respiration have been known for over 150 years: 1) respiration is regulated by a biological control system, and 2) under certain conditions an unsteady respiratory pattern may occur which is characterized by large oscillations about the mean ventilation, having a period of 15 to 60 seconds. This pattern is known as Cheyne-Stokes respiration (CSR). The primary hypothesis evaluated in this thesis is that CSR may be quantitatively accounted for by considering it to be a manifestation of unstable operation of the biological control system. A second major hypothesis studied, is that human respiratory control may exhibit a continuum of relative stabilities in which unstable or oscillatory behavior represents one extreme. These hypotheses are evaluated on both mathematical and experimental grounds. We shall now develop some of the historical and physiologic background which motivates the study of these hypotheses.

1.1. Cheyne-Stokes Respiration:

While it appears that under normal circumstances, human respiration is characterized by a steady pattern, even Hippocrates is believed to have described an oscillatory breathing pattern (1). The earliest formal description of Cheyne-Stokes Respiration came from J. A. Cheyne in 1818; "for several days his breathing was irregular; it would entirely cease for a quarter of a minute, then it would become perceptible,

though very low, then by degrees it became heaving and quick, and then it would gradually cease again. This revolution in the state of his breathing occupied about a minute during which there were about thirty acts of respiration" (2). This observation was made on a patient in severe heart failure, a condition which is now commonly associated with CSR (1,3). Figure 1.1a illustrates a classical CSR pattern as it typically occurs in patients with severe heart failure. Notice that the waxing and waning in ventilation occurs over a period of many breaths and that both rate and depth are oscillating.

It is now known that Cheyne-Stokes oscillations with a period of 20 to 30 seconds may occur in healthy individuals under a variety of circumstances. Figure 1.1b shows a breathing pattern which may be seen when normal adults are taken to high altitude (=5,000m). This pattern of ventilation can also be evoked by forcing healthy adults at sea-level to breathe gasses with abnormally low oxygen (O_2) concentrations (figure 1.1c). A number of other conditions have also been observed to induce CSR including; neurologic lesions, metabolic alkalosis, lung deflation, and increased circulation delays.

1.2. The Etiology of Cheyne-Stokes Respiration:

Since CSR was first described, its etiology has been debated. An important early hypothesis was that somewhere in the central nervous system there exists a self-sustained oscillator which under appropriate circumstances can dominate respiratory control (4). Though not universally accepted, contemporary support for this theory does exist (5,6,7,8). Part of the modern support for the existence of a single isolated oscillator derives from the fact that oscillations of identical

frequency have been observed in numerous biological parameters such as; ventilation, heart rate, blood pressure, sympathetic vascular tone, and splanchnic sympathetic tone.

Virtually all other theories regarding the etiology of CSR have been unified by the advent of control system modeling of respiration, and the suggestion that CSR may be a manifestation of unstable feedback control (1). This control system hypothesis has been explored by numerous investigators in the past 25 years, and many dozen mathematical models of CSR now exist. To appreciate this hypothesis, it must first be understood that human respiration is indeed a controlled behavior.

1.3. The Basic Operation of the Respiratory Control System:

The principal function of the human respiratory system is to supply adequate oxygen to the tissues, and to provide for the removal of the carbon-dioxide formed by cellular metabolism. To accomplish this function, the lungs are ventilated with fresh air from outside the body while circulating blood provides gas transport between the lungs and the tissues. By adjusting the rate of ventilation, the overall gas exchange requirements of the tissues can be met. It is in this context that respiration can be thought of as the output of a biological control system which detects the changing needs of the body and adjusts accordingly.

The essential elements of the respiratory control system are illustrated in figure 1.2a. While this representation is a simplification of known physiology, it is suitable for illustrating the operation of the control system. The respiratory centers of the rostral brainstem may be regarded as the controller of ventilation. The brainstem output, the

neural drive to breath, acts upon the inspiratory musculature to affect gas convection in the airways of the lungs.

This convection produces "alveolar ventilation" (\dot{V}_A), as it brings fresh air into the alveoli, which are the gas exchange areas of the lung. Diffusion equilibrium of oxygen and carbon dioxide (CO_2) occurs between the alveolar gas and the pulmonary capillary blood. This diffusion process allows blood passing through pulmonary capillaries to load O_2 and to unload CO_2 . The dynamics of this gas exchange determine the ongoing partial pressures of O_2 ($P_{a\text{O}_2}$) and CO_2 ($P_{a\text{CO}_2}$) in the arterial blood.

In order that $P_{a\text{CO}_2}$ may be regulated to a fixed setpoint, arterial receptors exist which can detect $P_{a\text{CO}_2}$ and relay this information neurally to the brainstem. This pathway completes a feedback loop by which \dot{V}_A may be regulated in order to maintain a relatively fixed $P_{a\text{CO}_2}$ despite changing metabolic demands or other disturbances. It is important to note that the $P_{a\text{CO}_2}$ receptors are not located within the lungs. They are therefore temporally separated from the gas exchange dynamics by a circulation transit delay. Thus the control system cannot respond instantaneously to any disturbance in gas exchange which occurs in the lungs.

While a number of feedback mechanisms have been described which are not included here, figure 1.2a illustrates the essential elements of respiratory control. These elements have been included in all mathematical models of CSR (9,10,11,12,13,14,15).

Figure 1.2b shows a linear model which may be used to describe respiratory control. The signal representing $P_{a\text{CO}_2}$ is detected and com-

pared to a setpoint value S . Their difference is the "error signal" which is acted upon by the controller, whose output represents \dot{V}_A . These operations reflect the actions of the receptors, the brainstem centers, and the inspiratory muscles of the biological system. A single controlled system element describes the gas exchange processes. The output of this element represents P_{aCO_2} . A pure delay element is used to model the biological circulation transit time.

Each of these model elements may be characterized by a transfer function; a complex quantity representing the gain and effective delay between input and output. The gain (or magnitude) of the controller transfer function is;

$$\text{magnitude of } A(f) = |A(f)| = \frac{d\dot{V}_a}{d(P_{aCO_2} - S)}$$

For the controlled system;

$$|B(f)| = \frac{dP_{aCO_2}}{d\dot{V}_A}$$

The pure delay has no effect on the signal amplitude such that;

$$|T_C(f)| = 1$$

The normal operation of this model is such that an equilibrium is achieved which is characterized by unchanging \dot{V}_A and P_{aCO_2} . As indicated in figure 1.2b, disturbances to this equilibrium may occur. For example, sighing and breath holding could be modeled as transient disturbances added to the controller output. Following a disturbance, a corrective action would be mediated by the control system in an attempt

to maintain the original equilibrium. The dynamics of this response are determined by the system stability, which we shall now define.

1.4. Stability Criteria

The model of figure 1.2b is said to be absolutely stable if for any bounded disturbance, the system response is also bounded. The conditions under which this model will display absolute stability may be defined mathematically in terms of the system loop gain, $LG(f)$;

$$LG(f) = A(f)B(f)T_c(f)$$

Loop gain is thus a complex quantity.

The relationship between $LG(f)$ and absolute stability is provided by the Nyquist criteria;

if at some critical frequency f_c , $LG(f_c)$ is a negative real number, then;

$$|LG(f_c)| < 1 \quad \text{absolutely stable}$$

$$|LG(f_c)| > 1 \quad \text{unstable}$$

That $LG(f_c)$ is negative and real requires that the angle of $LG(f_c)$ ($\angle LG(f_c)$) is -180° . Unstable operation is characterized by oscillations in \dot{V}_A and P_{aCO_2} at a frequency of f_c with an amplitude which increases with time. Thus the system response becomes unbounded. It is in this context that the sustained oscillations of CSR have been hypothesized to reflect unstable control system operation.

The binary concept of absolutely stable versus unstable model operation may be extended by asking; if the model operation is stable, how close is it to being unstable? To answer this question we may

define relative stability as a continuous measure of system behavior, one extreme of which is unstable operation. A number of measures of relative stability have been developed to describe physical control systems. A common technique is to use a feature of the system response to an impulsive disturbance as a continuous measure of relative stability. This technique is used in this thesis to characterize the relative stability of both mathematical and biological control systems.

For mathematical models, a fixed quantitative relationship exists between the loop gain and any impulse response measure of relative stability. For this reason, $|LG(f_c)|$ itself is often used as a measure of relative stability in mathematical models. The full range of relative stability is defined by;

$$0 < |LG(f_c)| < 1$$

$|LG(f_c)| = 0$ implies an absence of feedback and $|LG(f_c)| > 1$ implies unstable operation.

1.5. Mathematical Models of CSR: The State of the Art

As noted above, several mathematical models of CSR exist. These models have provided a single framework by which virtually all known causes of CSR may be interpreted. A potential mechanism has been described by which each cause of CSR could destabilize the control system, potentially creating oscillations. An excellent demonstration of this approach is provided in the model of Khoo et. al. published in 1982 (15). In many ways, the Khoo model represents the state of the art in modeling CSR. It is a single general model which can qualitatively account for the range of conditions under which CSR is known to occur.

It is also typical of existing models in many ways.

Figure 1.3 is a block diagram of the Khoo model. This model structure is considerably more complex than the one previously described. Note that multiple nested control loops and many system elements exist. In fact the transfer functions of some of these elements are dependent upon the signal values within the system. This level of complexity is typical of other CSR models (14,16,12,10). In addition, these models contain large numbers of parameters (e.g. Khoo et. al. = 18, Grodins et. al. > 30) which must be specified in order to constrain the model operation. Two significant problems derive from the complexity of these models; 1) the essential conceptual framework underlying the model stability may not be readily apparent and 2) they have not been quantitatively validated by direct experimental evidence.

1.5.1. Model Validation

The complexity of existing models of CSR makes it difficult or impossible to measure all model parameters in a single subject, in a single experimental setting. It is largely for this reason that quantitative comparisons between model behavior and experimental observations of CSR have been performed by employing "population normal" values for each model parameter. It is by this technique that mathematical models have been shown to exhibit unstable oscillations under conditions "typically" observed to induce CSR in "normal" adults.

The major problem with this approach is that the range of values seen in normal adults is significant for several important parameters. For this reason, employing normal parameter values does not constrain the model behavior sufficiently to allow a quantitative prediction of

respiratory control in any "normal" individual. No existing model of CSR has been validated by predicting the stability of respiration in a series of individuals.

In addition, the evaluation of existing models has focussed only on the unstable oscillations; under what conditions oscillations will occur and at what frequency. No systematic comparison of relative stabilities has been made between mathematical models and human respiration. Indeed, no systematic data exist regarding the relative stability of respiration under various conditions.

Evidence does exist which suggests that the tendency of the human respiratory control system to exhibit oscillations is a graded rather than an all-or-nothing phenomenon. For example, damped oscillations with a period similar to CSR are commonly observed following sighs in neonates(17,18) and adults at altitude (19). In addition, the strength of these oscillations depends on the operation of the control system (19). In that a sigh acts as an impulsive disturbance to the biological control system, these observations suggest that human respiration may exhibit a graded range of relative stabilities.

In addition, several investigators have reported that low amplitude non-random oscillations at the typical frequency of CSR exist in the resting breathing of both adults (20,21,22,23) and infants (24,17,18). It has been suggested that these oscillations reflect self-excitation of the system by biological noise sources (20,21,22,23,15). The variable amplitude of these oscillations may also indicate a variable relative stability of respiration.

1.6. Statement of the Problem

Two specific questions are answered in this thesis;

- 1) can a minimal model of human respiratory control be formulated which may be directly validated by experimental observations?

- 2) can this model accurately predict the relationship between $|LG(f_c)|$ and a quantitative measure of relative stability in a series of normal adults?

1.7. The Minimal Modeling Approach

In Chapter 2, a new model of human respiratory control is defined. This model is unique in that it represents an attempt to define the simplest mathematical model which is consistent with known physiology and retains the capacity to exhibit unstable behavior. This has been termed the "minimal modeling approach" (25) and offers several advantages over previous modeling attempts. First, only 6 physiologically distinct parameters are required to constrain the model operation. This greatly facilitates the validation of the model. In addition, to the extent that this minimal model can accurately predict the relative stability of human respiration, it can clearly illustrate the essential mechanisms which govern respiratory stability. In describing the structure of this model, expressions are derived for $LG(f)$ and f_c in terms of the 6 parameters. These expressions provide a direct mechanism for interpreting the effects of changing one or more physiologic parameters on the loop gain and hence the relative stability of the model. At the end of

Chapter 2 the quantitative relationship between $|LG(f_c)|$ and relative stability is illustrated. This relationship provides a prediction of the relationship which will be observed in the respiratory control of any individual.

1.8. Validation of the Minimal Model

Chapter 3 describes the experimental studies performed to determine the relationship between control system loop gain and relative stability in a series of healthy normal adults. The observed relationship is then quantitatively compared to that predicted by the minimal model. Despite the simplicity of the model, it is shown to accurately predict the relative stability of human respiration over a wide range of loop gains. The potential significance of this finding is also discussed.

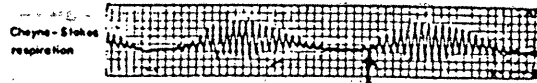
FIGURE CAPTIONS

Figure 1.1: a) Pneumographic recording of CSR illustrating regular waxing and waning of ventilation with periodically placed apneic periods of approximately equal length. Reproduced from Brown and Plum (3). b) Impedance plethysmographic recording taken from a sojourner at the 5400m Everest base camp in August 1981. The vertical bar indicates a 1 liter calibration and the upper tracing provides the time scale. Cycle duration is 20 s. Reproduced from Lahiri et. al. (19). c) Impedance plethysmographic recording from a healthy adult breathing 12% oxygen in nitrogen at sea level. Vertical scale is liters, time is seconds.

Figure 1.2: Block diagram representations of; a) the essential physiologic elements of the respiratory control system, and b) the equivalent representation of the linear control systems model.

Figure 1.3: Block diagram of the mathematical model of CSR published by Khoo and coworkers (15). Note that multiple nested control loops and many system elements are included in this model.

... ..
... ..
... ..



Everest base camp in August 1981. The vertical bar indicates a 1 min interval.

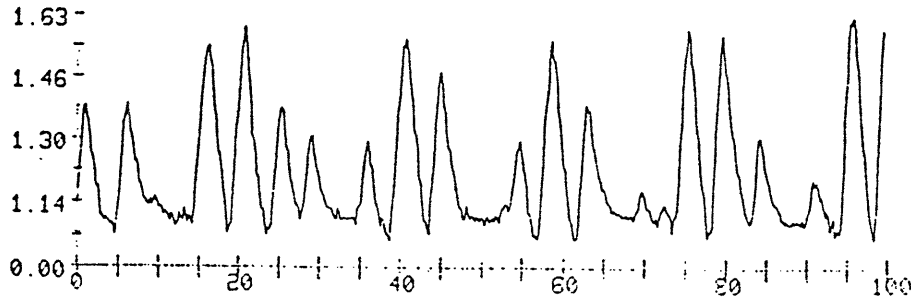
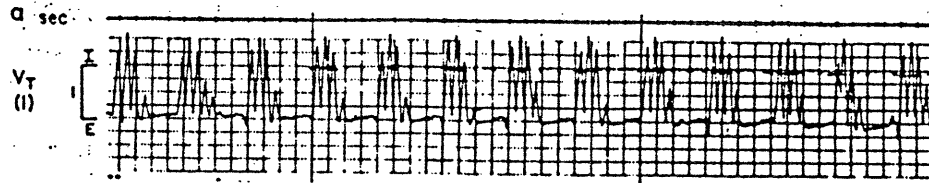


FIGURE 1.1

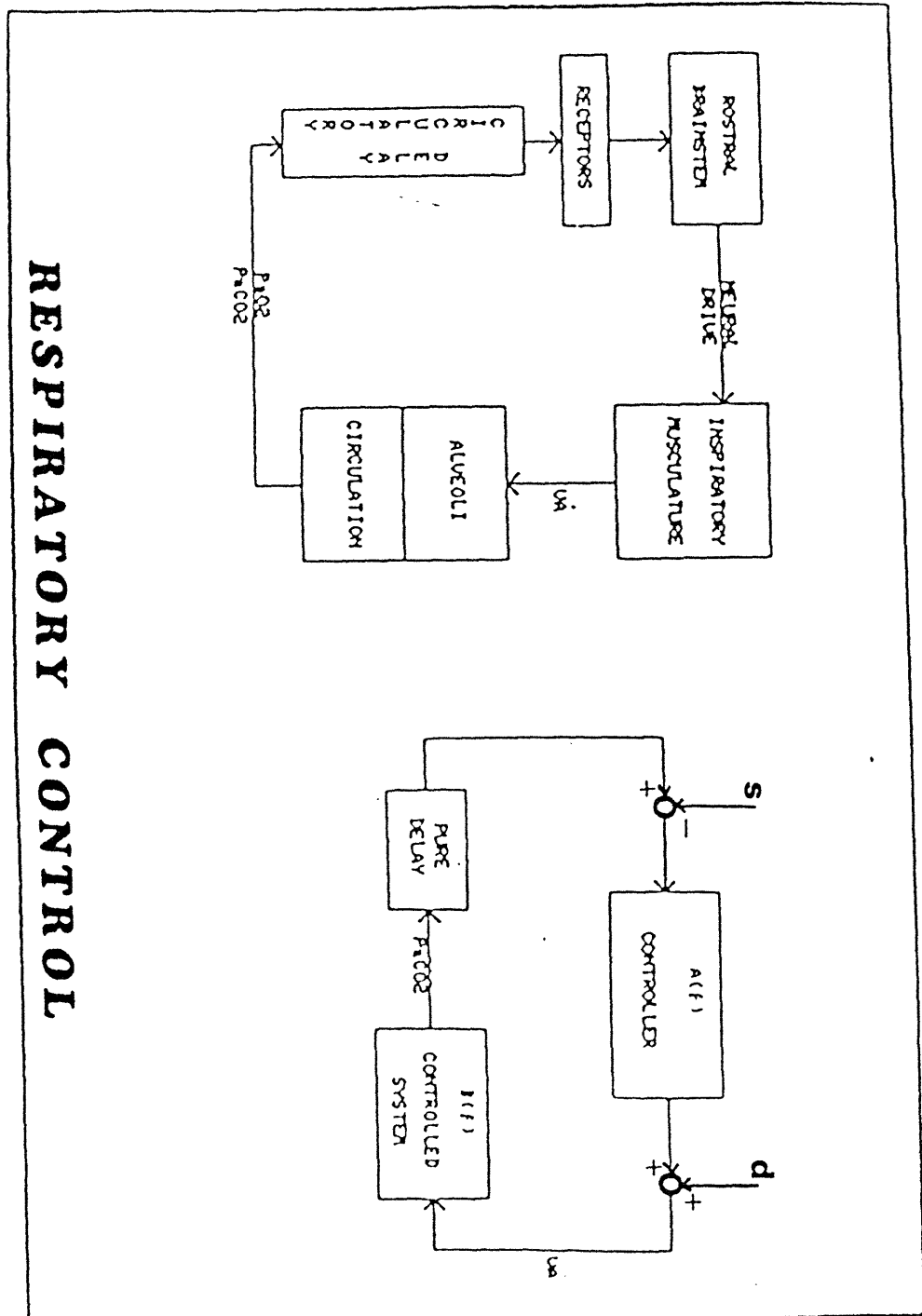
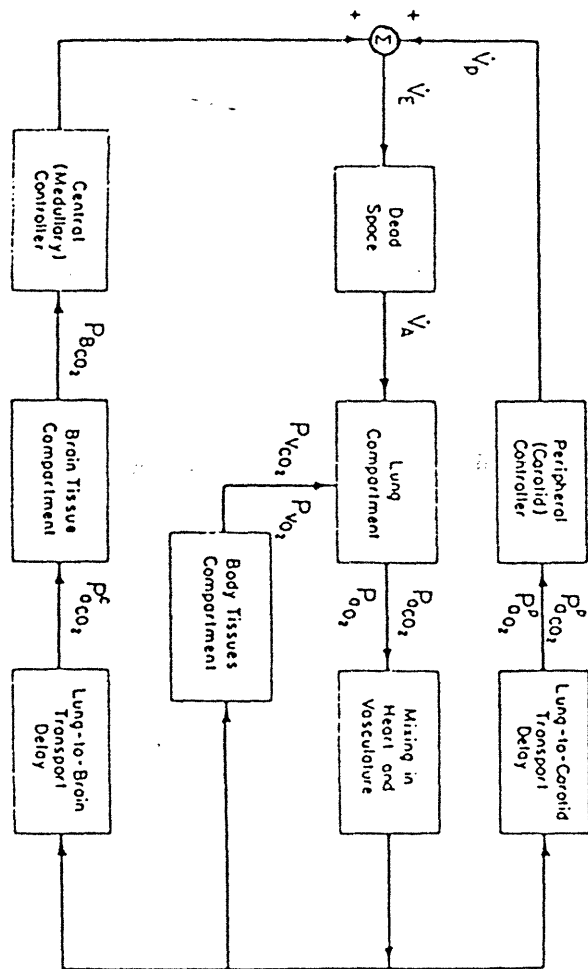


FIGURE 1.2



TYPICAL MODEL

FIGURE 1.3

CHAPTER 2

A MINIMAL MODEL OF HUMAN RESPIRATORY CONTROL

2.

2.1. Introduction:

In this chapter a new mathematical model of respiratory control is described. As noted in the introduction, an important goal has been to formulate a minimal model which is consistent with the physiology of respiratory control. For this reason, a number of simplifying assumptions and approximations to the physiology have been made and are explicitly stated. The expected range of validity for these assumptions is also discussed. The structure of the model is the single loop system described in the introduction. The mathematical formulation for the transfer function of each system element will be developed in terms of distinct physiologic parameters.

Although the biological control system is inherently non-linear, the model transfer functions are linear approximations. This linearization has two principal goals. First, the definition of absolute stability provided by the Nyquist criteria applies only to linear systems. The stability of the linear model is still quite informative, however. For the control system operation in the immediate vicinity of any equilibrium, an important theorem of Liapunov ensures that the underlying non-linear system is stable if and only if the linearized system is stable (26).

In addition, the formulation of linear transfer functions allows us

to derive an analytic expression for the loop gain. For this model, we shall show that $LG(f)$ is a function of 6 parameters which have clear physiologic counterparts. The analytic expression for $LG(f)$ allows a direct interpretation of the expected effects on loop gain of alterations in one or more physiologic parameters. The only previous linear model of CSR is that of Khoo et. al. (15). This group has clearly demonstrated the conceptual advantages of the linear approach over previous non-linear simulation models. Khoo et. al., however, made no attempt to formulate a minimal model which could be experimentally validated.

The expression for $LG(f)$ developed for the minimal model in this chapter forms a basis for the estimation of loop gain in human subjects. The 6 parameters which must be measured in each subject are clearly defined.

At the end of the chapter, we define the measure of relative stability employed in this thesis. The relationship between relative stability and $|LG(f_c)|$ is illustrated for the model. This model relationship provides a prediction of the same relationship for the human control system. In addition, a direct comparison is made between the minimal model and Khoo's model in appendix A 2. The effect of adding an isolated saturation nonlinearity to the model is described in appendix A 3.

2.2. The Minimal Model:

As indicated in the introduction, figure 2.1a represents the essential physiologic elements described by the model, while 2.1b is the minimal model diagram. The controller models the action of the P_{aCO_2}

receptors, the brainstem centers, and the inspiratory musculature and its output represents continuous alveolar ventilation. The controlled system of the model represents the airways, gas exchange surfaces, and vessels of the lungs. The controlled quantity is P_{aCO_2} and after a delay which models the circulation transit time, a signal proportional to this quantity is detected by the controller.

2.2.1. The Controlled System Transfer Function:

Although gas exchange in the lungs is distributed over a large number of alveoli, in healthy adults the ventilation and perfusion supplied to each alveolus is sufficiently uniform (21) that we may model the alveoli as a single well mixed gas space, and the pulmonary capillary blood as a single well mixed fluid space. If in addition we assume that constant temperature, pressure, and humidity are maintained in the gas compartment, then conservation of mass demands conservation of volume, yielding the Fick equation for CO_2 ;

$$\frac{dV_{ACO_2}(t)}{dt} = \tag{1.1}$$

$$\dot{Q}_c(t)(C_{vCO_2}(t) - C_{aCO_2}(t)) + \dot{V}_A(t)(F_{ICO_2}(t) - F_{ACO_2}(t))$$

where;

$V_{ACO_2}(t)$ = alveolar volume of CO_2

$\dot{Q}_c(t)$ = cardiac output

$C_{vCO_2}(t)$ = mixed venous CO_2 concentration

$C_{aCO_2}(t)$ = mixed arterial CO_2 concentration

$F_{ICO_2}(t)$ = inspired gas CO_2 concentration

$F_{ACO_2}(t)$ = alveolar CO_2 concentration

$\dot{V}_A(t)$ = continuous alveolar ventilation

t = time

... to this quantity is detected by the sensor...

Several assumptions will be made to simplify equation 1.1:

1) cardiac output is assumed to be constant;

$$\dot{Q}_C(t) = \dot{Q}_C \tag{1.2}$$

2) the relationship between CO_2 partial pressure and CO_2 concentration in the blood is assumed to be linear;

$$C_{CO_2} = K_{s1} P_{CO_2} + K_{s2} \tag{1.3}$$

where K_{s1} and K_{s2} are constants

3) P_{vCO_2} is assumed to be constant (we shall consider only local perturbations about an equilibrium);

$$P_{vCO_2}(t) = P_{vCO_2} \tag{1.4}$$

4) diffusion equilibrium occurs as blood traverses the pulmonary capillaries and no cardiac shunting occurs implying;

$$P_{ACO_2}(t) = P_{aCO_2}(t) \tag{1.5}$$

Combining eqs. 1.1 - 1.4 gives;

$$\frac{dV_{ACO_2}(t)}{dt} = \dots \tag{1.6}$$

$$\dot{Q}_c K_{s1} (P_{vCO_2} - P_{aCO_2}(t)) - \dot{V}_A(t) (F_{ACO_2}(t) - F_{ICO_2}(t))$$

In addition, from their definitions we know that;

$$F_{ACO_2}(t) = \frac{P_{ACO_2}(t)}{(P_B - P_W)} = \frac{V_{ACO_2}(t)}{mlv} \quad (1.7)$$

mlv = mean lung volume

$$F_{ICO_2} = \frac{P_{ICO_2}(t)}{(P_B - P_W)} \quad (1.8)$$

When eqs. 1.5 - 1.8 are combined we get equation 1.9;

$$\frac{dP_{aCO_2}(t)}{dt} = \frac{(P_B - P_W) (\dot{Q}_c K_{s1} (P_{vCO_2} - P_{ACO_2}(t)) - \dot{V}_A (P_{ACO_2}(t) - P_{ICO_2}(t)))}{mlv}$$

We may obtain the equilibrium expression relating P_{ACO_2} to \dot{V}_A by setting the time derivative in equation 1.9 equal to zero.

$$P_{aCO_2} = \frac{\dot{Q}_c (P_B - P_W) K_{s1} P_{vCO_2} + \dot{V}_A P_{ICO_2}}{(P_B - P_W) K_{s1} \dot{Q}_c + \dot{V}_A} \quad (1.10)$$

Equation 1.10 provides an equilibrium expression for the relationship between the controlled system input, \dot{V}_A and its output, P_{aCO_2} . Even when P_{ICO_2} is zero, this relationship is non-linear. Within the local vicinity of any initial operating point, we may satisfy our requirement for a linear transfer function by approximating equation 1.10 with the first two terms of its Taylor series expansion, obtaining;

$$P_{aCO_2} = \frac{-\dot{Q}_C(P_B - P_W)K_{s1}P_{vCO_2}}{(\dot{V}_A + \dot{Q}_C(P_B - P_W)K_{s1})} \frac{(\dot{V}_A - \dot{V}_A^o) + P_{aCO_2}^o}{2} \quad (1.11)$$

where,

$$\dot{V}_A^o, P_{aCO_2}^o = \text{initial equilibrium point}$$

Thus for incremental changes in equilibrium, the input/output relationship of the controlled system is given by;

$$\frac{dP_{aCO_2}}{d\dot{V}_A} = \frac{-\dot{Q}_C(P_B - P_W)K_{s1}P_{vCO_2}}{(\dot{V}_A^o + \dot{Q}_C(P_B - P_W)K_{s1})} \quad (1.12)$$

As demonstrated by Khoo et. al. (15), assuming typical adult values for each relevant parameter, if we consider P_{aCO_2} fluctuations of plus or minus 5 torr about the normal value of 40 torr, we expect less than a 10% error to occur in using eq. 1.12 to approximate the underlying hyperbolic relationship.

If we consider time varying, rather than steady-state departures from $\dot{V}_A^o, P_{aCO_2}^o$, equation 1.9 indicates that the gasses stored in the controlled system act approximately as a first order system. To obtain the time constant of this element we may solve the homogeneous form of 1.9;

$$\frac{dP_{aCO_2}(t)}{dt} + P_{aCO_2}(t) \frac{\dot{Q}_C(P_B - P_W)K_{s1} + \dot{V}_A}{mlv} = 0 \quad (1.13)$$

To see that;

$$T_0 = \frac{mlv}{\dot{Q}_C(P_b - P_w)K_{s1} + \dot{V}_A} \quad (1.14)$$

It is worth noting that identical results for $\frac{dP_{aCO_2}}{d\dot{V}_A}$ and T_0 can be obtained by the LaPlace transform technique if higher than first order terms are disregarded.

Extending the first order system analogy, we may write the transfer function for the controlled system as;

$$|B(f)| = \frac{B}{((2\pi fT_0)^2 + 1)^{.5}} \quad (1.15)$$

$$\angle B(f) = -\tan^{-1}(2\pi fT_0) \text{ radians} \quad (1.16)$$

2.2.2. The Controller Transfer Function:

The model controller is an instantaneous, linear, proportional controller. The input/output relationship of this controller is described by;

$$\dot{V}_A(t) = (P_{CR}(t) - S)A \quad (1.17)$$

where;

A = controller gain

$$P_{CR}(t) = P_{aCO_2}(t - T_C)$$

is the controller input

T_C = the delay magnitude

In equilibrium we have;

$$\dot{V}_A = (P_{aCO_2} - S)A \quad (1.18)$$

And the incremental equilibrium controller gain is;

obtained by the Laplace transform technique of higher order transfer functions

$$\frac{d\dot{V}_A}{dP_{aCO_2}} = A \quad (1.19)$$

Therefore the first order system is a constant gain controller.

As the controller is instantaneously acting, its transfer function is independent of frequency and is described by;

$$|A(f)| = A \quad (1.20)$$

$$\angle A(f) = 0 \quad (1.21)$$

In that this model includes only one feedback pathway, it represents an approximation of the human control system. It is well known that in man, separate CO_2 receptors exist in several locations.

- 1) Aortic Arch receptors exist which detect P_{aCO_2} and transmit afferent information through the vagus nerves.
- 2) Carotid Body receptors detect carotid arterial P_{CO_2} and P_{O_2} and relay this information through the carotid sinus nerves to the brainstem.
- 3) Brainstem receptors exist in the ventral medulla which are believed to respond to the P_{CO_2} of the cerebrospinal fluid bathing the brain.

The model controller is intended to represent only the concerted action of the carotid body receptors. The rationale for this is as follows;

- 1) careful studies of the response to changing P_{aCO_2} with and without intact vagus nerves indicate that aortic chemoreceptors are unimportant in human respiratory control.
- 2) both animal (27,28,29,30) and human (31,32,33,34) have indicated that brainstem receptors have little or no response to P_{aCO_2} oscillations at the typical frequency of CSR (f_c). Thus the brainstem receptors are not expected to contribute to $|LG(f_c)|$.
- 3) Although it includes no explicit description of the influence of P_{aO_2} on ventilation, the model is appropriate for simulating the relative stability of respiration in the immediate vicinity of any equilibrium level of P_{aO_2} . We feel that the significant decrease in model complexity justifies this limitation.

2.2.3. The Pure Delay Transfer Function:

The pure time delay has no effect on signal amplitude from input to output. It does, however, introduce a phase shift which is a linear function of frequency. The transfer function of this element is given by;

$$|T_c(f)| = 1 \quad (1.22)$$

$$\langle T_c(f) \rangle = -2\pi f T_c \text{ radians} \quad (1.23)$$

By using a fixed model delay, we have assumed that the circulation transit time remains constant.

2.3. Loop Gain of the Minimal Model

Recall that for a single loop linear system, the loop gain is defined as the complex product of the transfer functions around the loop. In this case;

$$LG(f) = A(f)B(f)T_c(f) \quad (1.24)$$

Equivalently;

$$|LG(f)| = |A(f)||B(f)||T_c(f)| \quad (1.25)$$

$$\langle LG(f) \rangle = \langle A(f) \rangle + \langle B(f) \rangle + \langle T_c(f) \rangle \quad (1.26)$$

Combining eqs. 1.15, 1.20, 1.22, and 1.25 gives;

$$|LG(f)| = \frac{AB}{((2\pi f T_0)^2 + 1)^{.5}} \quad (1.27)$$

Combining eqs. 1.16, 1.21, 1.23, and 1.26;

$$\langle LG(f) \rangle = -2\pi f T_c - \tan^{-1}(2\pi f T_0) \text{ radians} \quad (1.28)$$

2.4. Stability of the Minimal Model:

The absolute stability of the model may be evaluated using the Nyquist criteria. To do this, $|LG(f)|$ must be evaluated at $f = f_c$, where f_c is defined implicitly by;

$$\angle LG(f_c) = -180^\circ = -\pi \text{ radians} \quad (1.29)$$

Combining eqs. 1.28 and 1.29 yields;

$$f_c T_C + \frac{\tan^{-1}(2\pi f_c T_0)}{2\pi} = \frac{1}{2} \quad (1.30)$$

The absolute stability criterion for the model may thus be restated as;

$$|LG(f_c)| = \frac{AB}{((2\pi f_c T_0)^2 + 1)^{.5}} \geq 1 \quad \text{UNSTABLE} \quad (1.31)$$

Equation 1.31 indicates that $|LG(f_c)|$ is determined by the magnitudes of two dimensionless parameters;

AB: which may be regarded as the incremental equilibrium loop gain magnitude

$f_c T_0$: which determines the effective attenuation of the loop gain magnitude at the critical frequency

In addition, by combining eqs. 1.12, 1.14, 1.19, and 1.22 with eq. 1.31 we obtain the condition which must be satisfied (eq. 1.32) to produce unstable model behavior;

$$\frac{AP_{vCO_2} \dot{Q}_C K_{s1} (P_B - P_W)}{(\dot{V}_A^o + \dot{Q}_C K_{s1} (P_B - P_W))^2} \frac{1}{\left(\frac{(2\pi f_c m1v)^2}{(\dot{V}_A^o + \dot{Q}_C K_{s1} (P_B - P_W))^2} + 1 \right)^{.5}} \geq 1 \quad (1.32)$$

In addition;

$$AB = \frac{AP_{vCO_2} \dot{Q}_C K_{s1} (P_B - P_W)}{(\dot{V}_A + \dot{Q}_C K_{s1} (P_B - P_W))^2} \quad (1.33)$$

$$f_c T_0 = \frac{f_c mlv}{\dot{V}_A + \dot{Q}_C K_{s1} (P_B - P_W)} \quad (1.34)$$

The absolute stability criterion for the model may thus be restated

Equations 1.32 and 1.30 provide the relationships by which we have estimated $|LG(f_c)|$ in a series of human subjects, as described in the next chapter. We can see that in addition to monitoring ventilation, 6 parameters must be measured in each subject;

1) A

2) \dot{Q}_C

3) K_{s1}

4) P_{vCO_2}

5) mlv in the equation, in equation

6) T_C

According to this model, these 6 parameters are the essential determinants of the relative stability of respiration. We shall now illustrate the relationship between relative stability and $|LG(f_c)|$ for the model.

2.5. Relative Stability vs. Loop Gain:

The model relationship between $|LG(f_c)|$ and relative stability is

illustrated implicitly in figure 2.2. This family of waveforms depicts the controller output \dot{V}_A , as a function of time, and is parameterized by $|LG(f_c)|$. Each waveform comprises an initial constant \dot{V}_A characteristic of the equilibrium state, followed by the response to a 2.5s increase in P_{aCO_2} of 1 torr. It is readily apparent that with increasing $|LG(f_c)|$, both the amplitude and duration of the post-stimulus oscillations also increase. Note especially that for $|LG(f_c)| = 1.05$ the model is unstable, and the oscillation amplitude increases from cycle to cycle.

The waveforms of figure 2.2 indicate that for the model, \dot{V}_A is a continuous positive valued quantity which is constant at equilibrium. The equilibrium state of human respiration, however, is characterized by phasic fluctuations in lung volume and therefore \dot{V}_A . The controller output of the model may be considered a representation of the net alveolar ventilation which occurs with each breath in human respiration. The lack of a direct analogy between respiration and model output poses a problem for the following reason;

an important methodological constraint in validating the model predictions of relative stability is that both model simulations and experimental waveforms must be analyzed by identical signal processing techniques.

Experimental recordings of breathing patterns may be converted to continuous \dot{V}_A estimates of the same form as the model output. To do this, breath by breath estimates of \dot{V}_A could be computed from the experimental time series. This technique is undesirable for two significant reasons; 1) information regarding independent oscillations in the rate and depth of breathing is discarded and 2) the breathing rate is not

fixed so that the data samples are not uniformly spaced in time. The first consideration may cause a bias towards accepting model predictions of experimental observations and the second requires that different considerations be applied to the signal processing of model and experimental waveforms. It is readily apparent that with its

Instead of converting the data to the format of the model output, both the amplitude and duration of the post-stimulus oscillations we have converted the model output to the format of the data. This conversion in no way alters the functioning of the model; \dot{V}_A is preserved as an internal signal. However, the \dot{V}_A signal is used to generate an additional output which represent lung volume as a function of time ($v(t)$). This is done by decomposing \dot{V}_A into rate and depth components. The rate, or breathing frequency is chosen a priori and remains constant. Any fluctuations in controller output are then reflected as an amplitude modulation of the $v(t)$ waveform.

Figure 2.3 uses $v(t)$ to illustrate relative stability in the style of figure 2.2. The P_{aCO_2} disturbance occurs on the third "breath" of each waveform. The breathing frequency chosen here is .2 Hz, which is typical of adult respiration. Note that equilibrium is characterized by a non-sinusoidal waveform. In fact, this "carrier" waveform is the absolute value of a sine wave with a frequency of .1 Hz. The "absolute value" sine wave was chosen to provide a phasic pattern more closely analogous to the physiologic waveform. Although the absolute value function is a non-linear operation, it is employed solely in the generation of the lung volume output. It neither introduces a non-linearity into the control loop, nor invalidates the model expressions derived for transfer function. This technique is unproblematic for the significant $LG(f)$ and f_c .

2.6. Defining the Measure of Relative Stability:

Figures 1.2 and 1.3 have illustrated the relationship between the system response to an impulsive disturbance and the value of $|LG(f_c)|$. As indicated in the introduction, many specific measures of relative stability based on the impulse response have been applied to physical control systems. For example; peak amplitude of the first cycle, time after disturbance of the first peak, and effective damping coefficient are commonly used. Because the human control system is not truly a second order system, and because it contains significant random variability, or noise, we have sought a more robust measure of relative stability. We have defined the low frequency power of the impulse response as our measure of relative stability.

The logic of this measure is illustrated in figure 2.4 which depicts the power density spectrum of the impulse response at $|LG(f_c)| = 1.05$ (figure 2.3). The distribution of power for this waveform is dominated by two peaks. The high frequency peak, centered at .2 Hz arises from the phasic nature of the equilibrium waveform, and by analogy to modulation may be regarded as the "carrier peak". The lower frequency peak, centered at equilibrium waveform. It is the power of the low frequency which is the basis of our measure of relative stability. The protocol for calculating the relative stability from a transient response waveform is as follows.

- 1) Two time series are obtained and sampled at .2s intervals; a) the prestimulus epoch = 102.4s of ventilation waveform obtained immediately after the onset of the disturbance, and b) the post-stimulus epoch = 102.4s of ventilation waveform obtained immediately after

the onset of the disturbance (which we shall refer to as the stimulus).

2) The power density spectrum of each waveform is computed using smoothed periodogram techniques. (See Appendix 1 for a description of the technical details and their significance).

3) The total power of the carrier peak (centered at the mean breathing frequency) is computed for the pre-stimulus spectrum.

4) Both pre-stimulus and post-stimulus spectra are normalized by the total power of the pre-stimulus carrier peak. This controls for the direct effect of carrier power on disturbance induced low frequency power.

5) The normalized pre-stimulus spectrum is subtracted from the normalized post-stimulus spectrum. This difference describes the normalized redistribution of power, or power induced by the stimulus.

6) The power at all frequencies is normalized by the peak magnitude (in torr) of the disturbance. This controls for the direct influence of stimulus amplitude on the low frequency power of the system response.

7) The measure of relative stability, low frequency power, is defined as;

$$\text{low frequency power} = \frac{\int_{.01\text{Hz}}^{.1\text{Hz}} \text{power}(f)df}{.1\text{Hz}} \quad (1.35)$$

Here, power(f) is the normalized function of frequency obtained after

step 6 of the above protocol.

Low frequency power is a measure of relative stability based on the power of the "envelope" oscillations induced by a transient disturbance. This measure is robust in that it is relatively insensitive to minor deviation from linear second order system behavior which may be induced by random variability or non-linearity in the biological control system. In addition, as appropriate normalization has been employed, the magnitude of low frequency power will be sensitive only to $|LG(f_c)|$. Most importantly, identical signal processing techniques may be employed in evaluating low frequency power from model and experimental waveforms. In fact, the numerical values for intersample interval and epoch duration have been based on experimental constraints as described in the next chapter.

Figure 2.5 illustrates the relationship between low frequency power and $|LF(f_c)|$ (labeled loop gain). Notice the sigmoid nature of this relationship. For $|LF(f_c)|$ less than approximately $|LG(f_c)| = .5 - .6$, a "knee" occurs and low frequency power increases rapidly with increasing $|LG(f_c)|$. This knee may be regarded as analogous to the transition from overdamped to underdamped behavior. Only for the underdamped case is the system response oscillatory.

Figure 2.5 forms a prediction for the same relationship in human respiration. This prediction is quantitatively validated in the next chapter. Appendix 2 contains a detailed evaluation of the minimal model using population normal parameter values. The conceptual value of considering $|LG(f_c)|$ in terms of 2 dimensionless parameters is demonstrated. A detailed comparison to the model of Khoo et. al. (15) is also provided. Appendix 3 explores the use of describing function

analysis to allow the analytic description of a single saturation non-linearity to be included in the model. This saturation is motivated by the observation that physiologically, \dot{V}_A must be non-negative. Including this non-linearity allows fixed amplitude oscillations analogous to periodic breathing to be modeled for $|LG(f_c)| \geq 1$.

of which nature, or non-linearity in the biological control system

the system is not linear, and the system is not linear.

the system is not linear, and the system is not linear.

the system is not linear, and the system is not linear.

the system is not linear, and the system is not linear.

the system is not linear, and the system is not linear.

the system is not linear, and the system is not linear.

the system is not linear, and the system is not linear.

the system is not linear, and the system is not linear.

the system is not linear, and the system is not linear.

the system is not linear, and the system is not linear.

the system is not linear, and the system is not linear.

the system is not linear, and the system is not linear.

FIGURE CAPTIONS

Figure 2.1: Block diagram representations of; a) the essential physiologic elements of the respiratory control system, and b) the equivalent representation of the linear control systems model.

Figure 2.2: Illustration of model response to a 2.5s 1 torr disturbance in P_{aCO_2} for various values of $|LG(f_c)|$. All waveforms are plotted on a common abscissa. The time scale is provided by the 10s bar. The ordinate for each waveform is \dot{V}_A as scaled by the .51 bar. Note that both the strength and duration of the oscillations in \dot{V}_A increase with increasing $|LG(f_c)|$. For $|LG(f_c)| = 1.05$, the model is unstable, as indicated by the growth of the oscillation with time.

Figure 2.3: Implicit illustration of relative stability versus $|LG(f_c)|$ in the format of figure 2.2. In this case, waveforms represent $v(t)$ rather than \dot{V}_A . The disturbance occurs on the third "breath" of each waveform.

Figure 2.4: Power density spectrum of model response to 2.5s 1 torr disturbance in P_{aCO_2} for $|LG(f_c)|$. Abscissa is frequency (Hz) and the ordinate is power density. Note the resolution of the impulse response into 2 distinct frequency components. The higher frequency peak arises from the phasic nature of the equilibrium pattern. The lower frequency peak arises from the modulation of the equilibrium pattern induced by the disturbance.

Figure 2.5: Relationship between low frequency power and $|LG(f_c)|$ for

the minimal model. Note the sigmoid shape of this function. A 'knee' exists in the region of $|LG(fusbc)| = .5$.

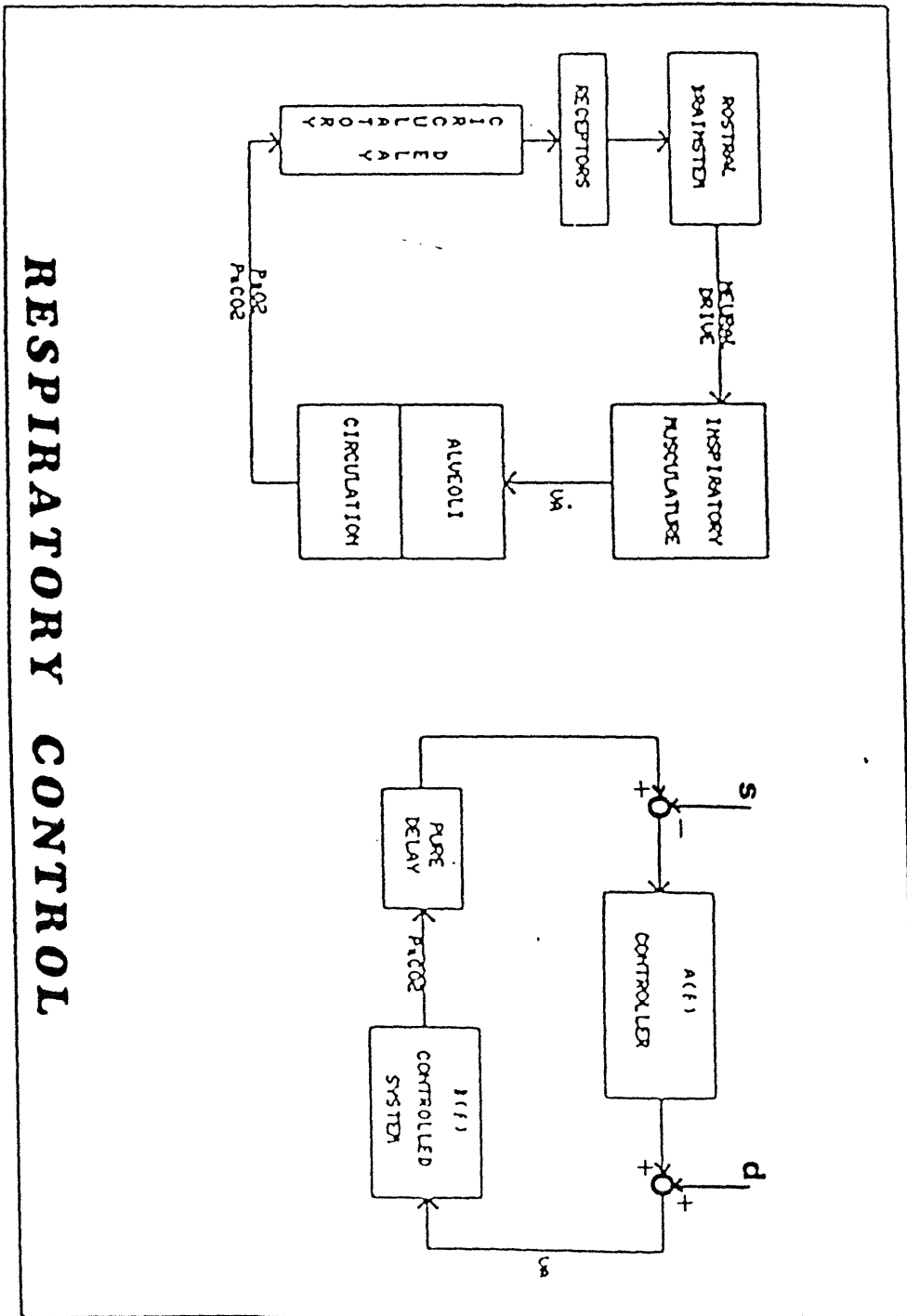


FIGURE 2.1

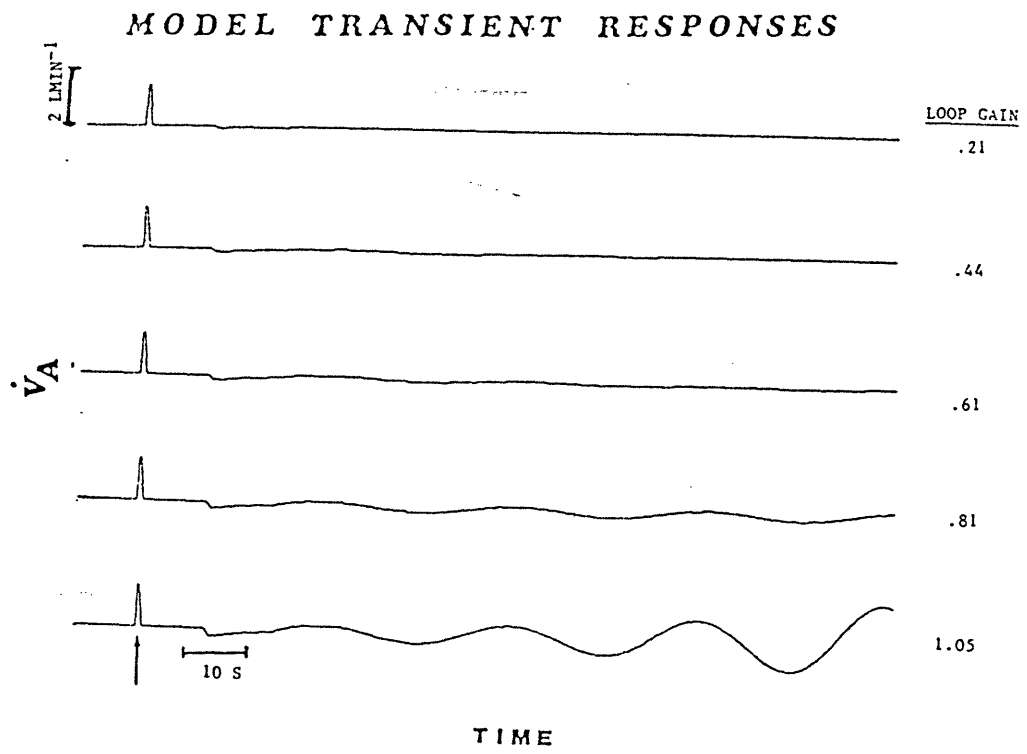


FIGURE 2.2

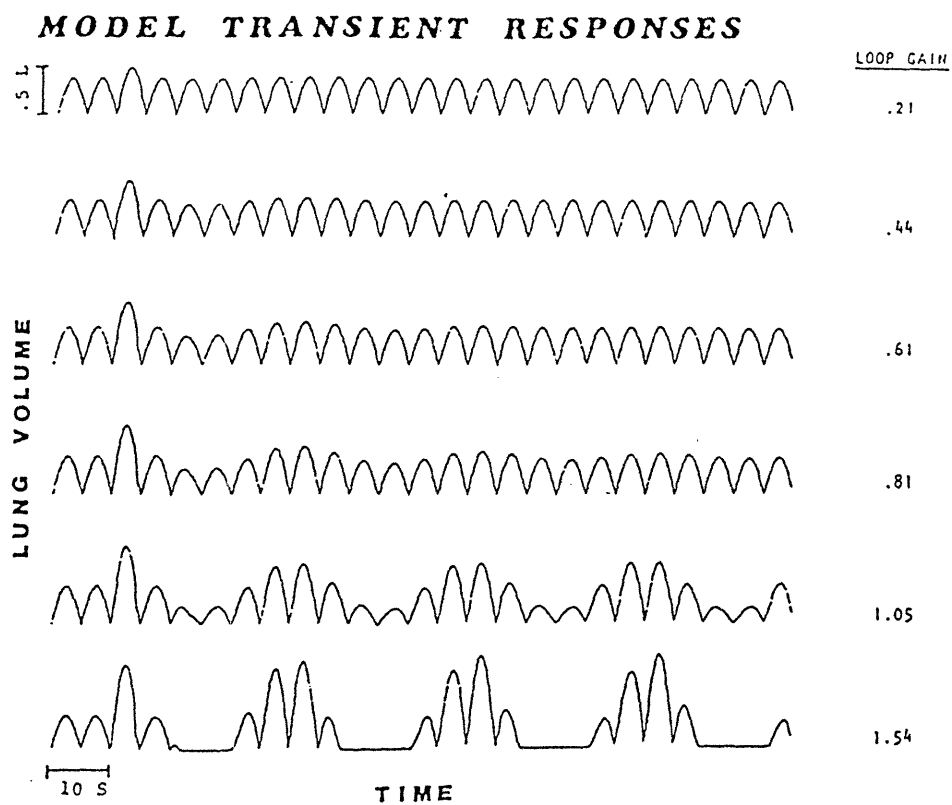


FIGURE 2.3

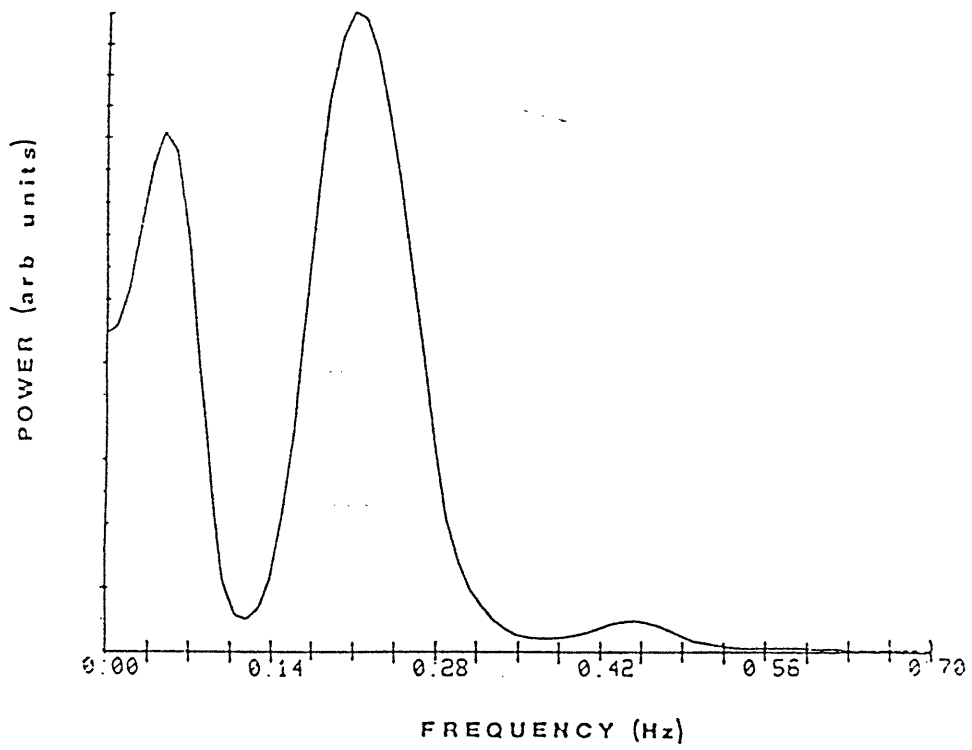


FIGURE 2.4

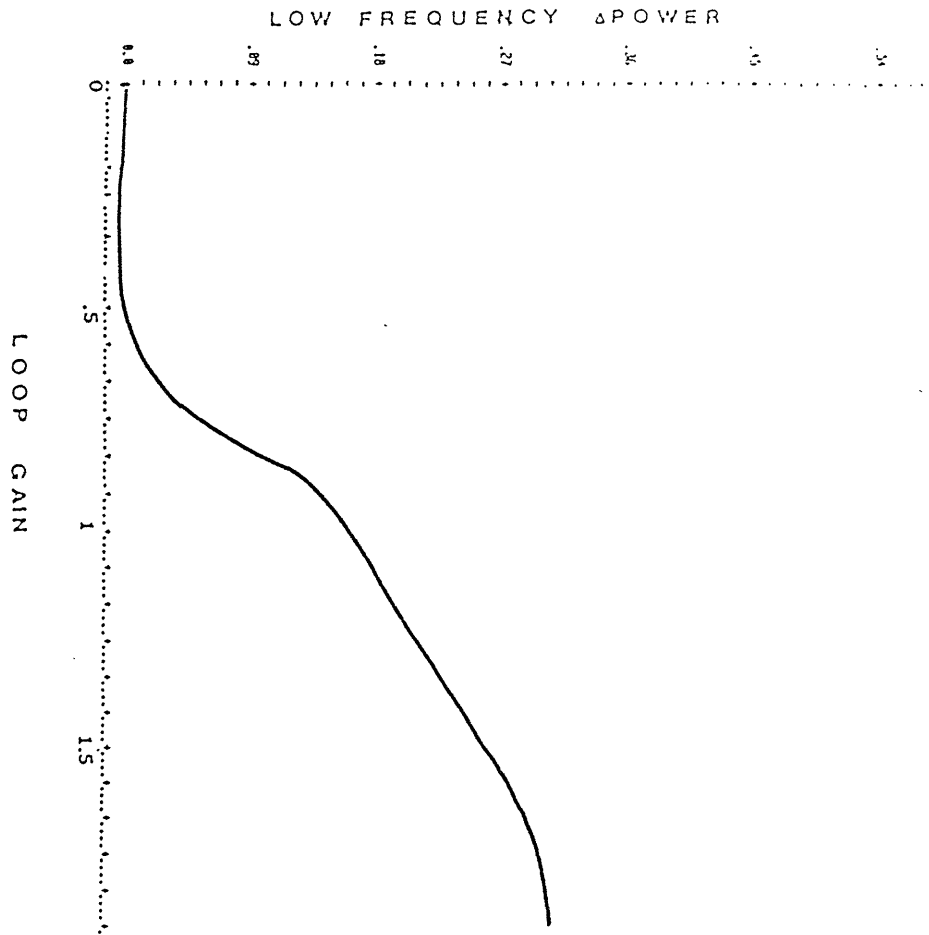


FIGURE 2.5

CHAPTER 3

VENTILATORY RESPONSES TO TRANSIENT PERTURBATIONS OF ALVEOLAR
CO₂ DURING GRADED HYPOXIA IN MAN

3.

3.1. Introduction:

As described in the introduction, under certain conditions, the breathing of healthy adults can follow an oscillatory pattern which closely resembles Cheyne-Stokes respiration (CSR). For example, this type of CSR may occur; 1) following voluntary hyperventilation (35) , 2) at high altitude (36,19,37) and 3) during sleep (38). A common link between these conditions is a degree of arterial hypoxemia; and indeed hypoxemia has been postulated as a potent cause of CSR (35,19,37,38,1,39,36).

Control systems modeling of respiration has provided the insight that an increase in sensitivity of the CO₂ control mechanism caused by hypoxemia (40,41,42,19,43,44,45,31,46) may cause an instability in respiratory control (39) demonstrated by oscillatory breathing. In fact, simulation studies have shown that mathematical models of respiratory control can qualitatively account for virtually all conditions known to induce CSR in animals (47,16) and humans (9,14,12,15,16). The implication of this finding is that whenever CSR occurs, it is a manifestation of instability in the biological control system. The behavior of these models also suggests that human respiration may be

characterized by a continuous relative stability, one extreme of which represents unstable operation.

While these implications are quite provocative, no mathematical model of CSR has been quantitatively validated. As previously described, it is the complexity of these models which has prevented their direct validation. In the previous chapter, a minimal model of respiratory control was described. The loop gain ($LG(f)$) and hence the relative stability of this model is constrained by 6 physiologically distinct parameters. In addition, the low frequency power was defined as a measure of relative stability which could be applied to human respiration. Finally, the model relationship between low frequency power and loop gain magnitude ($|LG(f_c)|$) was demonstrated. This relationship forms a prediction of the relative stability of respiration in any individual based on the $|LG(f_c)|$ for his control system.

In this chapter, we shall describe the methods by which we have determined the relationship between relative stability and $|LG(f_c)|$ in 15 healthy normal adults. In each study, measurements were made of each parameter necessary to characterize $|LG(f_c)|$. In addition, a series of transient disturbances were induced in order to assess the low frequency power. These measurements of $|LG(f_c)|$ and low frequency power were repeated at several levels of background hypoxia. The objective of this protocol was to characterize the relative stability of respiration at several loop gains in each subject by taking advantage of the well known hypoxic potentiation of the CO_2 sensitivity (and hence $|LG(f_c)|$).

Finally we demonstrate that the observed relationship between relative stability and loop gain is quantitatively predicted by the minimal mathematical model. The implications of this finding are discussed.

3.2. METHODS

3.2.1. Apparatus:

The experimental apparatus used in these studies has two basic roles; 1) to manipulate the inspired gas composition in order to induce steady-state changes in P_{aCO_2} and P_{aO_2} and short duration, impulsive disturbances in P_{aCO_2} and 2) to record all relevant baseline and respiratory response data. The first function is served by seating the subject in a comfortable armchair and positioning a hood over his head to the shoulder level (figure 3.1). A known mixture of O_2 , N_2 , and CO_2 is passed first through a humidifier (cascade; Bennet), and then into the upper end of the hood. The total gas flow rate is maintained at a minimum value of 2.0 ls^{-1} and a baffle is used to distribute this flow uniformly over the cross section of the hood. The O_2 concentration of the mixture is continuously monitored at the inlet to hood (model 5575; Ventronics).

It is our interest in studying the pattern of ventilation which has motivated the use of this gas delivery system rather than the more common face-mask or mouthpiece apparatus. Direct evidence exists which demonstrates dramatic alterations in the steady-state breathing pattern when adults at rest breathe via masks or mouthpieces(48). It is believed that this may be a result of oral mucosal stimulation and or mechanical loading of the respiratory system. Both of these situations are obviated by the use of the hood, although slight trigeminal stimulation may be caused by gas convection.

Four signals are recorded simultaneously on a polygraph (model 78D; Grass) and on a magnetic tape (3968A Instrumentation Recorder; Hewlett Packard) later replayed for analysis by digital computer (VAX-11/750; Digital Equipment); ECG, airway P_{CO_2} , transcutaneous P_{O_2} , and instantaneous lung volume. The electrocardiographic activity is monitored using silver silver-chloride electrodes in a lead I configuration. Airway P_{CO_2} is monitored by infrared absorption (model PM-20NR; Cavitron). The response time of this instrument (< 150 ms) is suitable for monitoring end-tidal gasses in adults. A transcutaneous P_{O_2} electrode (TCM-2; Radiometer) is placed in the left supraclavicular fossa. Respiration is monitored by inductive plethysmography (Respirace Corp.) using both thoracic and abdominal transducers. Numerous quantitative validations of this technique have been published (49,50,51). This instrument is calibrated for each study, employing the simultaneous equation technique of Watson(52). This calibration is checked in a sitting position before the hood is placed and again at the end of each study. For recording purposes, we select a final 1 volt per liter signal level.

3.2.2. Experimental Protocol:

We have performed the following protocol on each of 15 adult male volunteers (age = 24.3 ± 1.7) from whom full informed consent had been obtained. The health of each subject was established by a negative history for neurologic and cardiovascular disease and chronic or acute respiratory disease. In addition, performance on standard flow-volume maneuvers was evaluated. The functional residual capacity of each subject was measured by whole-body plethysmography (body plethysmography

system; Warren E. Collins).

At the start of each study the subject was comfortably seated (as in figure 3.1) and allowed to rest quietly. A CO_2 sampling cannula was positioned superficially in one of the ala nasi. After the end-tidal CO_2 partial pressure has stabilized (visual inspection of the polygraph record), 2 minutes of quiet breathing were recorded in order to characterize the resting minute ventilation, P_{ACO_2} and CO_2 excretion.

The remainder of the experimental protocol is illustrated in figure 3.2; where time is shown on the abscissa and the inspired gas composition is indicated by the ordinates. At the start of each study, the subject breathed room air (21% O_2 and 0% CO_2) and a series of measurements was made in order to characterize the equilibrium gain and time constant of the controlled system (B and T_0 , respectively). Recall from equations 1.12 and 1.14, that in order to evaluate B and T_0 , the following parameters must be measured; cardiac output, mixed venous P_{CO_2} , the mean lung volume, the solubility of CO_2 in blood, and the water vapor pressure in the alveolar gasses.

The following rebreathing maneuver allowed P_{vCO_2} and \dot{Q}_C to be estimated. With a nose-clip in place, the subject breathed deeply and rapidly through a mouthpiece into a closed, 800 ml bag for 30 seconds. During this interval, no CO_2 excretion occurred, and the gasses of the lungs and the bag equilibrated with mixed venous blood. By measuring the P_{CO_2} of the bag before significant recirculation from the tissues occurred, we obtained an indirect measure of P_{vCO_2} . This maneuver represents only a slight modification of the rebreathing technique of

Campbell and Howell (53). Figure 3.3 illustrates the maneuver and the corresponding CO_2 waveform seen in the bag. As we shall later describe, the equilibrium Fick equation for CO_2 was then used to provide an indirect measure of cardiac output.

The hood was next positioned over the subject's head and ventilated with room air. The subject was asked to relax using the hood as a head-rest. Miniature headphones were provided for listening to soft classical music. The remainder of the protocol required approximately 90 minutes.

A minimum of 10 minutes was allowed for the subject to reach a steady-state breathing pattern under the hood, in a bias flow of room air. The inspiratory CO_2 concentration was then briefly elevated to a peak of approximately 4%. This created a transient disturbance in the equilibrium between \dot{V}_A and $P_{a\text{CO}_2}$. The response to this disturbance was used to characterize the relative stability of respiration as described in Chapter 2. Figure 3.4 illustrates a typical transient response sequence. The first half of this record represents normal resting breathing and will be referred to as the pre-stimulus epoch. The post-stimulus epoch begins with the first inhalation of elevated P_{CO_2} and also lasts 102.4s. The direct effect of the stimulus lasts from 2 to 5 breaths, and creates a peak elevation in end tidal P_{CO_2} of 2 to 10 torr. A minimum of 2 minutes following the post-stimulus epoch was allowed for respiration to return to baseline. This transient stimulation was performed from 2 to 4 times. No stimulus was applied at a time when sustained ventilatory oscillations could be observed on the polygraph

record.

Following the final transient response, the CO_2 sensitivity was determined as a measure of the subject's controller gain. To do this, the inspired CO_2 concentration was raised to approximately 4%. This F_{ICO_2} was maintained for 3 minutes. The final 2 minutes of this period were used to characterize the CO_2 response. This CO_2 response measurement is similar to rebreathing techniques in that 3 minutes is insufficient time for the body tissues to equilibrate with the elevated F_{ICO_2} . For this reason, P_{vCO_2} , and hence P_{aCO_2} rise slowly during the final 2 minutes of this protocol. The rate of this rise, however, is slow with respect to the speed of response of the arterial chemoreceptors (54,55,56,57). The adequacy of this technique to provide an appropriate measure of chemosensitivity for the study of transient responses is demonstrated in the discussion section of this chapter.

The challenges and measurements described thus far are sufficient to allow both the loop gain of the control system, and the relative stability of respiration to be estimated. Both the transient and steady-state CO_2 responses were then repeated at F_{IO_2} 's of 15% and 12%, with the objective of measuring relative stability at higher loop gain magnitudes. A 10 minute equilibration period was allowed after each change in F_{IO_2} before a new series of CO_2 responses was recorded following the protocol outlined above. After the final steady-state CO_2 response recording, the hood was once again ventilated with room air for 10 minutes and the protocol was terminated.

3.2.3. Analysis Procedures:

The data were digitized by replaying the tape through a 6 pole Butterworth filter (corner frequency = 10 Hz), and sampling at 40 per second. The digitized data were then convolved with a 31 point finite impulse response low pass filter (corner frequency = 2 Hz), and every 8th sample was stored. The effective sampling rate is 5 per second. The digital filtering in the final step was non-causal and the only phase shift appeared in the form of a pure delay which affected all signals uniformly. Calibration information recorded at the time of the study provided the scaling factors for the airway P_{CO_2} (torr) and instantaneous lung volume (liters) signals.

3.2.3.1. Loop Gain Calculations:

Recall from Chapter 2 that we wish to determine the relationship between $|LG(f_c)|$ and relative stability for each subject. In this section, we describe the calculations by which $|LG(f_c)|$ was estimated.

3.2.3.1.1. The Controlled System:

We shall now describe the method by which the controlled system gain was estimated, where;

$$|B(f_c)| = \frac{P_{vCO_2} \dot{Q}_C k_{s1} (P_B - P_W)}{(\dot{V}_A^o + \dot{Q}_C K_{s1} (P_B - P_W))^2 \left(\frac{(2\pi f_c m l v)^2}{(\dot{V}_A^o + \dot{Q}_C K_{s1} (P_B - P_W))^2} + 1 \right)^{.5}}$$

The recordings necessary to evaluate this expression were made at the

start of each study. Two minutes of resting breathing were used to estimate; \dot{V}_A^o and \dot{V}_{CO_2} . \dot{V}_{CO_2} and the dead space volume, V_D were estimated using a modification of the Douglas-bag technique:

Ten liters of exhalatory gas were collected at the beginning of the response low pass filter (corner frequency = 2 Hz) and a 2 minute interval, and the total collection time was noted. The

CO_2 volume fraction (F_{CO_2}) of this gas was measured in order to

calculate \dot{V}_{CO_2} by:

$$\dot{V}_{CO_2} = \frac{F_{CO_2} \times 10}{\text{collection time (s)}} \text{ l s}^{-1}$$

In addition, the end-expiratory P_{CO_2} was determined for each breath in the collection interval by visual inspection of the airway P_{CO_2} record. The mean P_{ACO_2} was estimated as the mean end-expiratory P_{CO_2} for all breaths during the collection. The mean expiratory tidal volume (V_T) was taken as $10/N$ liters, where N was the number of breaths. The dead space was estimated as;

$$V_D = V_T \left(1 - \frac{P_{CO_2}}{P_{ACO_2}}\right)$$

Finally, the mean \dot{V}_A was calculated as;

$$\dot{V}_A = \frac{10 \times \left(1 - \frac{V_D}{V_T}\right)}{\text{collection time}} \text{ l s}^{-1}$$

The rebreathing protocol described above was used to estimate $\dot{Q}_c (K_{s1})$ as;

$$\dot{Q}_{Cs1}^K = \frac{\dot{V}_{CO_2}}{(P_{vCO_2} - P_{ACO_2})}$$

As cardiac output and CO₂ solubility always appear together as a product, we have no need to estimate them independently.

The barometric pressure was measured by mercury manometer at the time of each study. The water vapor pressure of the alveolar gasses was assumed to have a normal value of 47 torr. From the measurements outlined above, we calculated |B(.044Hz)|, where .044Hz was the mean critical frequency observed over all subjects. |B(.044Hz)| was assumed to be constant throughout each individual study. To complete the estimate of |LG(.044Hz)|, the controller gain, A was evaluated.

3.2.3.1.2. The Controller:

The value of A was measured from the response to steady-state CO₂ breathing at each F_{IO₂} in each study. Breath by breath analyses of 2 data epochs were performed for each response; 1) a 2 minute control epoch ending at the onset of increased F_{ICO₂}, and 2) a 2 minute response epoch beginning 1 minute after the onset of increased F_{ICO₂}. The value of A was calculated as;

$$A = \frac{\dot{V}_A}{P_{ACO_2}} = \frac{\dot{V}_A^R - \dot{V}_A^C}{P_{ACO_2}^R - P_{ACO_2}^C}$$

superscript R = response epoch

superscript C = control epoch

These values of A were combined with the controlled system calculations

to obtain estimates of $|LG(.044)|$ at each level of hypoxia in each study.

3.2.3.2. Relative Stability Calculations:

As previously indicated, the responses to transient disturbances in P_{aCO_2} were used to characterize the relative stability of respiration in these studies. All transient responses were identified and analyzed according to the methods described in Chapter 1, subject to the following exclusion criterion; neither the pre-stimulus nor the post-stimulus epoch of any transient response was coincident with those of any other transient response. Such coincidence was not a problem for the planned disturbances. However, spontaneous sighs also induce transient disturbances on P_{aCO_2} with a magnitude similar to those induced as part of the protocol. Both induced and spontaneous transient responses were analyzed subject to the above exclusion criterion. Each acceptable response was analyzed in order to determine the power(f) function and the low frequency power. The signal processing techniques employed in these calculations are precisely the same as those employed in analyzing the model responses in Chapter 2. These methods are described in detail in Appendix 1. Eighty five transient responses have been analyzed from the 15 studies.

In order to illustrate the average characteristics of power(f) obtained from these 85 responses, one additional step has been taken. For each response, the frequency axis of power(f) is normalized by the mean breathing frequency of its own pre-stimulus epoch. All 85 power(f) functions were rank ordered by their corresponding values of these values of a wide combined range of controlled variables.

$|LG(.044Hz)|$ and divided into six ranges. The average power(f) was then computed for each range.

3.3. Results:

3.3.1. Baseline Results:

Table 2.1 presents the values of the baseline parameter estimates obtained from each subject during resting breathing of room air. The range across subjects of each parameter and of $|LG(.044Hz)|$ is typical of normal adults. These results are presented primarily for comparison to previous work.

3.3.2. Power(f) versus $|LG(f_c)|$: Model Results

Figure 3.5 presents the normalized power density spectrum of the phasic model output observed during the pre-stimulus or equilibrium state. This figure is a 3 dimensional projection plot of power density against loop gain magnitude and normalized frequency. The 6 values of $|LG(f_c)|$ correspond to the means of the six groups of experimental responses. It is readily observed in figure 3.5 that the relative distribution of power in frequency is not a function of $|LG(f_c)|$. At each loop gain, the spectrum is dominated by a single peak. This peak is centered at a normalized frequency of 1 due to the normalization.

Figure 3.6 illustrates the distribution of power in the post-stimulus model output. In contrast to figure 3.5, note the presence of substantial power at frequencies of less than half the mean breathing frequency. This power arises from the low frequency oscillations in

ventilation following the disturbance, and increases with increasing loop gain. Only at the highest loop gain does any obvious redistribution of power occur in the vicinity of the control breathing frequency. The actual change in power distribution between pre- and post-stimulus epochs is defined by the power(f) function, which is presented in figure 3.7. This figure clearly demonstrates that significant low frequency power is added to the model output in the post-stimulus epoch. This power increases with loop gain magnitudes of greater than approximately .5. For lower loop gains, no significant redistribution of power occurs at any frequency.

3.3.3. Power(f) versus |LG(.044Hz)|: Experimental Results

Eighty five transient responses have been analyzed. In order to present the average response characteristics as a function of loop gain, these transients have been pooled into loop gain ranges as indicated in figure 3.8. The cutoffs of each range are noted at the top of the figure. The histogram of individual loop gains within each range is presented in the middle of the figure, and the descriptive statistics for each range are listed below the histograms.

Figure 3.9 presents the average pre-stimulus spectra as a function of loop gain. As for the model, the average power spectrum is not systematically dependent on the average loop gain. Each of the 6 average spectra is characterized by a single carrier peak. No significant power exists aside from this peak. In addition, the morphology of this peak shows no obvious dependence on loop gain.

The dependence of the average post-stimulus spectrum on loop gain is seen in figure 3.10. A major difference between pre- and post-stimulus spectra is that significant low frequency power exists in the post stimulus spectra, which increases with loop gain magnitude. There also exists a significant carrier peak at each loop gain. These peaks are not centered precisely at unity, but the location does not appear to be systematically dependent upon loop gain. The width of the peak is broader than the corresponding pre-stimulus peak at all loop gains. Inspection of individual spectra reveals that this broadening results primarily from a variable location of the carrier peak in the post-stimulus spectra. Averaging the individual spectra then creates the broadening seen in figure 3.10. In addition, note that the carrier peaks at the two highest loop gains contain significantly more power than their corresponding pre-stimulus peaks.

Figure 3.11 presents the average power(f). At low loop gains, little power has been added to the ventilation spectra by the perturbations. Deviations from baseline for loop gains less than .5 represent minor changes in the morphology of the carrier peak. As the loop gain increases further, significant, systematic spectrum changes do occur, however. The same unit of perturbation adds significant power to the spectrum. This power appears at dimensionless frequencies; 1) below .4, and 2) in the immediate vicinity of 1. The power added in each of these regions increases with increasing loop gain. This figure provides direct evidence that the power of the ventilatory response to transient P_{aCO_2} perturbations is; graded, frequency specific, and strongly dependent on loop-gain. In addition, a comparison of figures 3.7 and 3.11 indicates that each of these features is as predicted by the behavior of

the minimal model. It should again be emphasized that identical signal analysis techniques were employed in analyzing both model and experimental waveforms. This 3 dimensional format is useful for illustrating one additional point; the distribution of power in resting ventilation as a function of $[LG(.044Hz)]$. control peak to peak loop gain. Intra de

3.3.4. Power Density Spectra of Resting Ventilation:

In addition to the transient responses just described, 13 epochs of sustained spontaneous oscillation were identified. The operational definition of these epochs was; at least 10 visible cycles in ventilation must occur, for which the mean peak to trough change in minute ventilation for the last 5 cycles must be as great as the mean for the first 5 cycles. Seven epochs of sustained oscillation occurred during resting ventilation, including 2 epochs with $F_{iO_2} = 21\%$. The remaining 6 epochs were triggered by transient perturbations. These six epochs have been included in the analysis of transient perturbations. If we include the 7 control epochs of sustained oscillation with the set of pre-stimulus epochs, the result is depicted in figure 3.12. This figure presents the tendency of the system to display self-excited oscillations at different loop gains. In contrast to figure 3.9, note the significant increase in low frequency power with increasing loop gain. This result indicates that the occurrence of spontaneous oscillations may indeed be regarded as the result of self-excitation, and that their power may be understood in terms of the relative stability of the control system.

The three dimensional plots described above afford an excellent

means of examining the distribution of ventilatory power as a function of loop gain. They provide a direct visual basis for making feature comparisons between model and experimental responses. However, only average experimental behavior is illustrated. In addition, it is difficult to illustrate quantitative comparisons in this three dimensional format. As defined in Chapter 2, the low frequency power is a more suitable quantitative basis of comparison.

3.3.5. Low Frequency Power versus $|LG(f_c)|$:

A plot of low frequency power vs loop gain for all 85 transients is presented in figure 3.13. Transients from different studies are coded by different letters. Coincident points are plotted as asterisks. Treating all points equally, a correlation coefficient of $R = .83$ is obtained between low frequency power and the loop gain estimates at .045 Hz. This verifies a significant relationship between these two quantities even when no averaging is performed. In addition, performing a linear regression yields an intercept of $-.07$ and a slope of $.23$, as a description of this relationship.

Figure 3.14 highlights the correlation between low frequency power and loop gain within each experiment. To obtain this plot from figure 3.13, a single point was computed for each gain estimate in any experiment. The value of low frequency power for each such point was taken as the average low frequency power of all transients analysed from that hypoxic steady-state. Points from each study are connected by line segments. This slight degree of averaging improves the correlation to $R = .88$ without changing the regression significantly ($p < .05$). Note also

that low frequency power tends to increase with increased loop gain within each study as well as over the entire data set. A one-way analysis of variance on the six data groups described in figure 3.8, also indicates that low frequency power is significantly dependent on loop gain magnitude ($P < .0001$).

Figure 3.15 presents the model prediction, superimposed on figure 3.14. Good agreement is seen between the model behavior and the data points. In fact, an inflection point in the data is suggested by the knee in the model curve. In order to test the degree of fit between the model prediction and the experimental data, the residual errors were examined. Analysis of variance indicates that the mean error is not a function of loop gain magnitude. The mean error over all loop gains, however, has a value of .039 and is significantly greater than zero ($p > .05$). This error represents approximately 10% of the low frequency power observed at the highest loop gains.

3.4. Discussion:

The results just described provide the first direct evidence that the tendency of the respiratory control system to oscillate under both free and forced excitation is quantitatively linked and in a graded fashion, to the relative stability of the equilibrium operating point. Although it has long been known that transients such as sighs may precipitate oscillations, this is the first systematic demonstration that such induced periodic breathing is only an extreme case of the response to transient CO_2 disturbances which occurs under conditions of low relative stability. These results indicate that both spontaneous and

induced oscillations in respiration may be quantitatively accounted for by the dynamic operation of the control system. While our findings do not exclude the existence of self-contained oscillators in the central nervous system (5,7,4) , they do indicate that such oscillators need not exist in order to account for ventilatory oscillations induced by hypoxia. In addition to these major conclusions, several specific points merit further discussion.

3.4.1. F_{IO_2} versus Controller Gain:

Table 2.1 describes the average controller sensitivity to CO_2 for F_{iO_2} of 21%, 15%, and 12%. The hypoxic potentiation of A indicated in this table is consistent with many previous observations, but the magnitude of the sensitivity at each F_{iO_2} is approximately half of the typical values reported by Edelman et. al. (46). There are several possible sources for this discrepancy. First, the sensitivities reported in figure 3.5 are for changes in alveolar ventilation, while the values reported by others are typically for changes in expiratory ventilation. However, we have computed expiratory sensitivities as well, and this factor accounts for only 30% of the discrepancy.

Another factor is that we have not determined true steady-state sensitivities. Our response epoch is taken from the second and third minutes of CO_2 breathing. While this time is sufficient for alveolar equilibration, it is insufficient for tissue equilibration(58,59,10,15). In fact, Khoo et. al. (15) estimate that the normal time constant for equilibration in brain tissue is 80 seconds. Thus at the time we begin

our response measurement, the brainstem chemoreceptors are not contributing their full steady-state response. This may be an important factor, as the central chemoreceptors are believed to contribute greater than 50% of the normal CO_2 sensitivity even under mild hypoxia (31,32). The sensitivity measurements reported by Edelman and others have allowed sufficient time for full equilibrium responses to occur.

Another factor which could decrease the magnitude of our measured

sensitivity is that isoxic conditions were not rigidly maintained during CO_2 breathing. Although the mean P_{ACO_2} elevation was less than 5 torr, the increased alveolar ventilation creates a slight increase in P_{AO_2} . This elevation in P_{aCO_2} should reduce the measured response somewhat. We cannot quantitatively evaluate this effect as direct monitoring of P_{aO_2} was not available.

One final factor which may have influenced the sensitivities we measured is the gas distribution system. An important design criterion of this system was that that no mechanical contact with the airways be imposed. Such contact is known to influence steady-state breathing patterns (48) and may also influence steady-state sensitivity. Any such influence would be absent from our measurements.

Of the factors outlined above, the most significant is probably the fact that in our protocol, the central receptors reach only a fraction of their equilibrium response. For our purposes, however, this is desirable. In characterizing the ability of the controller to support self-sustained oscillations, we need to know the sensitivity to oscillations which occur every 20 seconds. The speed of response of the

central receptors is so slow that they undoubtedly contribute little sensitivity to such oscillations. If our arterial steady-state sensitivity measurements contain any significant portion of central response, we might expect them to overestimate the appropriate sensitivity. Indeed, several studies have shown that the controller sensitivity at frequencies of several per minute is significantly less than the full steady-state sensitivity (34,33,31).

In order to assess the validity of using arterial steady-state responses to characterize the controller response to an oscillatory P_{ACO_2} , we developed a technique of estimating the controller sensitivity at the frequency of the oscillation for each transient response analysed. The basis of this technique is as follows;

- 1) breath by breath sequences for end-tidal P_{CO_2} and \dot{V}_A are computed.
- 2) These sequences are then expanded back to real time by according each value a number of points equal to the duration of that breath in the original time series.
- 3) The relative delay from CO_2 waveform to ventilation waveform which maximizes the positive cross-correlation is determined. This delay is usually between one and two breaths, and is inferred to be equal to the circulation delay.
- 4) After applying this delay, the cross and auto spectra are computed and employed to determine the transfer function between P_{ACO_2} and \dot{V}_A , assuming ventilation to be the dependent variable.

- 5) The magnitude of the transfer function at the frequency of transient ringing is taken to be the controller sensitivity.
- 6) This controller gain estimate may then be combined with B_0 and T_0 to obtain the appropriate loop gain estimate.

Figure 3.16 is a plot of this cross correlation loop gain estimate (cclg) is plotted against the corresponding steady-state loop gain estimate (sslg) for all 85 transients analyzed. The correlation coefficient between the two estimators is .95. The linear regression has a slope which is not significantly different from unity ($p > .05$), and an intercept which is not significantly different from 0 ($p > .05$). Thus, for the purposes of estimating the transient response sensitivities, sslg and cclg are equivalent estimators. Given this result, there are two major advantages to our use of the steady-state estimates to describe the data.

First, from a methods viewpoint, it is superior to use the steady-state estimates. In this way, one set of experimental procedures is performed to constrain the model and a completely separate set of procedures is performed to evaluate its predictive capacity. Using the cross correlation technique entails estimating a model parameter and then evaluating the ability of the model to account for the same data.

The second advantage to using the steady-state sensitivity estimates is statistical. the estimation uncertainty associated with cross correlation estimator may be substantial. It is straight forward to show that when this technique is used to estimate transfer functions, the relative uncertainty in the magnitude is proportional to $(1 - c^2)$,

where c is the coherence between the two signals (60). For a linear transfer function in a deterministic system, c is unity. However, in biological systems, c may be reduced by both nonlinear system behavior, and the presence of random variability. For the transient epochs analyzed here, the range of c^2 is .13 to .91. This is similar to the experience of others (18,61). For the epoch in which c^2 is .13, the 75% confidence interval is 150% of the estimate. Although the steady-state technique provides no frequency specific information, the estimation uncertainty is considerably smaller.

The conclusion of this analysis is that despite certain uncontrolled factors which may affect the steady-state sensitivity, this technique provides a good estimate of the controller sensitivity to transient excitation. This finding strongly reinforces the conclusion that the minimal linear model evaluated, accurately predicts the response to experimental transients. Let us now turn to a discussion of the response spectrum data.

3.4.2. Interpretation of Power as a Function of Loop Gain:

The frequency domain was chosen to describe the experimental data because we are considering inherently oscillatory phenomena. It should be noted, however, that the frequency resolution is limited to $\pm .0049$ Hz. The oscillations we are describing have a characteristic frequency of approximately .05 Hz. Although it would otherwise be desirable, higher resolution can be obtained only by analyzing longer data epochs. This is not practical in this study for two reasons; 1) if we apply local perturbations, only at the highest loop gains studied do the responses last even 2 minutes, and 2) especially at low F_{i0_2} movement,

coughing, sighing, and other behavioral responses occur with sufficient frequency that it is difficult to obtain artifact-free responses many minutes in duration.

Because of the limited low frequency resolution, response epochs following sighs begin with the breath immediately after the sigh. As a large ventilatory transient, if the sigh is included, it introduces low frequency power beyond the resolution of the analysis. This power "leaks" into the frequency range which is analyzed, corrupting out spectrum estimates at the frequencies of greatest interest. Several other points must be made regarding the interpretation of figure 3.10.

Consider the distribution of power between frequencies of .4 and 1.0. In contrast to the model behavior (figure 3.7) the power in this range is non-zero. It has already been noted that part of this power derives from the variable distribution of the post-stimulus carrier peaks. A second consideration is that if the location of the low frequency peak is uncorrelated to the location of the control epoch carrier peak, some smearing of the low frequency power will occur due to the frequency normalization. This will tend to broaden the low frequency peak in the average spectra. A third influence, especially at high loop gains, is the possible occurrence of modulation induced side lobes about the carrier peak in the post-stimulus spectrum. Such additional peaks do in fact occur in a few individual spectra, but this phenomenon is not resolved in the average spectra.

3.4.3. Model Simulations:

Consider the equilibrium waveform of the phasic model output (fig-

ure 2.4). This waveform is obtained by taking the absolute value of a sine-wave at one half of the mean breathing frequency. This has the effect of creating an asymmetric "one-sided" modulation based on the controller output. This type of modulation is in fact analogous to the physiologic situation in which tidal volume oscillates above a relatively fixed functional residual capacity. Making the model carrier correspond to this situation has a significant impact on the spectral characteristics of the model transient responses.

Simple modulation theory shows that if a .25 Hz sine wave is multiplicatively (amplitude) modulated by a .05 Hz sine wave, the spectrum of the resulting waveform will contain power only at .2 Hz and .3 Hz. The absolute value function has the effect of demodulating the waveform in order to recover the 2 original frequencies. This implies that the low frequency power seen in physiologic transient responses is linked to this asymmetric modulation. The principal value of deriving this output from the linear model is that identical analysis techniques may then be applied to both simulated and experimental responses. This greatly facilitates the quantitative comparison between model predictions and the data.

3.4.4. Comparing Model Prediction and Experimental Observations:

We have performed a comparison between model behavior and experimental data based on low frequency power; the normalized power between .01 and .10 Hz. This is desirable as it reduces the estimation error associated with the computed power density at any single frequency. This parameter also has the benefit of being relatively insensitive to the precise period of the oscillation.

As described above, our only estimates of the circulation delay derive indirectly from optimizing the cross-correlation between the P_{ACO_2} and \dot{V}_A waveforms of each transient. For this reason, we have not employed the model relationship (eq. 1.30) to predict the critical frequency in our studies. Instead, we have employed the mean oscillation frequency over all 85 transients of .045Hz as the critical frequency in all cases. This is justified by the fact that if we evaluate the location of the low frequency peak as a function of either, loop gain or F_{iO_2} , no significant correlation is found ($p < .05$).

The important conclusions to be drawn from comparing the model predictions to the experimental observations are that;

- 1) a significant relationship exist between the relative stability of human respiration and the loop gain of the respiratory control system; and
- 2) a minimal linear control system model can completely account for the dynamics of this relationship

3.4.5. Implications for Other Models:

Much of the value in this model's ability to predict transient response behavior stems from its minimal implementation. Under conditions of steady-state hypoxia, this model provides analytic relationships to describe the relative stability which are sufficient to predict the conditions under which transient and sustained ventilatory oscillations will occur on an individual basis.

As our model is based on the same basic principles as most existing models of CSR, these models may also successfully account for the experimental data presented here. Some caution is well advised in making this conclusion, however. Our model incorporates what we consider to be a minimum set of elements essential in modeling relative stability. We describe only one control loop, one single pole low pass element and one pure delay. As more elements and pathways are added, the resulting model may predict response features which are not supported by the data.

For example, the linear model Khoo et. al. (15) includes a circulation delay which is dependent upon P_{ACO_2} . Due to this dependence, they predict a normal adult oscillation period of 30s for $F_{iO_2} = 21\%$ and 21s for $F_{iO_2} = 12\%$. Our data, as shown in figure 3.24 demonstrates a mean cycle time of 22.13s for $F_{iO_2} = 21\%$ and 22.6s for $F_{iO_2} = 12\%$; a difference does not achieve statistical significance. Thus the more complicated model would erroneously predict a decreasing cycle time with progressive hypoxia. This dependence of cycle time does appear to be consistent with the observations of Waggener et. al.(37) on spontaneous oscillations at altitude. It may be that when sustained CSR is allowed to develop, interaction between P_{AO_2} and cycle time becomes more prevalent.

3.5. Conclusions:

The experimental results reported in this chapter provide direct evidence that under conditions of progressive hypoxia, the power of ventilatory oscillations induced by transient disturbances provides a measure of relative stability which is strongly correlated to the loop gain

of the control system. This characterization can be extended to include both spontaneous and transient induced oscillations. Sustained oscillations may be understood and predicted on a basis of control system instability. The smooth increase in low frequency power with increasing loop gain magnitude coupled with the observation that transient disturbances can initiate sustained oscillations at high loop gains indicates that sustained oscillations represent an extreme case of the transient response, rather than a separate phenomenon.

In addition, we have shown that a minimal control system model can account for the behavior described above. This model accurately predicts the low frequency power in the transient responses of a series of individuals over a range of relative stabilities spanning more than an order of magnitude. This predictive ability further supports the hypothesis that both damped and sustained respiratory oscillations are a reflection of control system dynamics. In addition, this model provides analytic expressions describing the relative stability of the control system which accurately account for the experimental data.

3.5.1. Significance of Results:

The results and conclusions described above indicate that models of respiratory control can provide an effective means of distinguishing between ventilatory oscillations which reflect control system operation from those which do not. This fact may have clinical significance in several regards. For example, sleeping infants commonly exhibit periodic breathing (24,17,18,62,63). It is believed, however, that this periodic may have multiple etiologies and abnormalities in periodic

breathing have been linked with the sudden infant death syndrome (62,63). In addition, adult sleep apnea syndromes often present periodic ventilatory events of uncertain etiology. The minimal mathematical model described in this thesis may be useful in distinguishing periodic apneas which are a result of excessive loop gain from those which are not.

The findings of this thesis are also of significance to our general understanding of respiratory physiology. They indicate that while human respiration contains significant random variability, the deterministic aspects of respiratory dynamics are indeed dominated by the action of the feedback system under physiologic conditions.

3.5.2. Suggestions for Future Work:

Several direct extensions of this work are suggested by the results presented in this thesis. First, given that the minimal model accurately predicts the relative stability of human respiration indicates that the analytic expression for loop gain derived in Chapter 1 is a valid approximation under physiologic conditions. This expression then forms the basis of precise predictions of the effects varying one or more physiologic parameters on the relative stability of respiration. The range of validity for these predictions may be rigorously evaluated with the use of suitable animal models. Clinical studies designed to investigate the etiology of periodic apnea could also be framed around the minimal model. We are currently beginning a study of periodic breathing and apnea in patients with familial dysautonomia, a disease which effects general autonomic function.

Additional modeling work is also suggested by our results. A

significant limitation in the utility of the minimal model in investigating the etiology of various oscillatory phenomena is related to the controller characterization. A large body of evidence indicates that no discrete control element exists in the body which directly regulates alveolar ventilation. Instead, it appears that inspiratory effort, inspiratory duration, and expiratory duration are all regulated on a breath to breath basis based on a dynamic interaction of peripheral and central elements. A mathematical model which emulated the known pathways in this physiologic control schema more directly may be of significantly greater potential utility in evaluating the etiology of oscillatory phenomena. We have formulated and are currently evaluating such a model, which is the first of its kind. While the simulation behavior of this model may provide important insights, its complexity is comparable to previous models of CSR. It may prove possible, however, to quantitatively validate this model through the use of appropriate animal studies.

FIGURE CAPTIONS

Figure 3.1: Schematic representation of the gas delivery system used in these studies. The subject rests in a lounge chair and the open ended hood is positioned his head. This hood is ventilated with a bias flow of the desired composition. The inspiratory gasses of the subject are drawn from the bias flow, and have the same composition. The expiratory gasses are also cleared by the bias flow. The bias flow composition is manipulated by jet mixing of oxygen, nitrogen, and carbon-dioxide. This mixture is humidified before entering the hood.

Figure 3.2: Schematic illustration of the experimental protocol. Time is illustrated in minutes on the abscissa, and inspiratory gas composition is given by the ordinates for F_{IO_2} and F_{ICO_2} .

Figure 3.3: a) This figure illustrates the rebreathing maneuver performed to estimate the mixed venous carbon-dioxide tension. Starting from quiet breathing, the subject makes a normal inspiration and then exhales to fill a closed .8 liter bag. He then breathes from this closed system for a minimum of 30 seconds. b) The typical CO_2 waveform obtained from the sampling cannula in the mouthpiece. Note that the first exhalation illustrates the resting alveolar carbon-dioxide tension. As rebreathing continues, the alveolar gas equilibrates with venous blood, and the respiratory oscillations disappear from the waveform. This plateau reflects the mixed venous carbon-dioxide tension.

Figure 3.4: Lungvolume and airway P_{CO_2} waveforms from a typical induced transient perturbation. The transient begins at time = 100s. The

direct effects of the perturbation last 4 - 5 breaths, but visible ringing in both lung volume and end-tidal P_{CO_2} continue through the end of the record.

Figure 3.5: Three dimensional projection plot of the power density spectrum for the model pre-stimulus, or equilibrium breathing pattern as a function of loop gain. The baseline table is tipped toward the viewer, and is formed by the loop gain (.21 - 1.54) axis and the frequency (0 - 2.8) axis. The vertical axis is normalized power density (see text for details regarding the computation of these spectra). Hidden lines are not removed. Note that the spectrum morphology is independent of loop gain due to the normalization by the area of the carrier peak (see text).

Figure 3.6: The spectrum characteristics of the model post-stimulus breathing epoch as a function of loop gain. Notice the addition of significant low frequency power at high loop gains.

Figure 3.7: The power spectrum response of the model as a function of loop gain. Note that no significant change in the carrier peak occurs, but that a separate low frequency peak arises for loop gains greater than approximately .6.

Figure 3.8: Side by side histograms and descriptive statistics indicating the division of the transient epochs into loop gain ranges, for averaging purposes.

Figure 3.9: Three dimensional projection plot of the average spectrum characteristics for 85 transient perturbations. This surface represents the average power spectrum of the control epochs in each loop gain

range. Note the similar morphology of the carrier peak at each loop gain.

Figure 3.10: Three dimensional projection plot on the same coordinates as figure 3.9. This surface represents the average spectrum characteristics of the post-stimulus epochs within each loop-gain range. Note the somewhat variable position and increased width of the carrier peaks with respect to the spectra of the control epochs. In addition, note the presence of significant low frequency power, especially at high loop gains.

Figure 3.11: Three dimensional surface representing the average power spectrum response in each loop gain range. No significant response is seen at any frequency for loop gains below approximately .6. For greater loop gains, power is added in the region of the carrier peak, and in a separate low frequency peak.

Figure 3.12: Three dimensional projection plot the the average spectrum characteristics of the control epochs of the 85 transients. In addition, 7 epochs of spontaneous, sustained oscillatory ventilation have been included in the data set. Note that for loop gains greater than approximately .8, significant low frequency power exists.

Figure 3.13: A scatter plot of the low frequency power versus the loop gain magnitude for 85 transients. A significant correlation exists between these two parameters. The linear regression equation is also provided below the plot.

Figure 3.14: Same axes as figure 3.13. One point is plotted for each unique value of loop gain for each study. The average low frequency

power is plotted for each loop gain magnitude within each study. Solid lines connect the points from each study. Note that the correlation between these two parameters exists within each study, not only in the pooled data.

Figure 3.15: Scatter plot of the same data as figure 3.14. The solid line represents the minimal model prediction of this relationship.

Figure 3.16: Scatter plot of cross-correlation loop gain estimates versus steady-state loop gain estimates, for 85 transients. A correlation of $R = .95$ exists between these 2 estimators.

CASE NO. LABEL	1 VA	2 PACC2	3 PCCO2	4 VCCO2	5 DC	6 VD	7 frc	8 E8	9 T8	
1	3.420	38.900	46.900		.187	5.500	.132	3.730	-1.950	18.600
2	3.530	37.100	47.300		.183	4.500	.119	3	-2.200	18.900
3	7.060	40.300	47.800		.398	12.600	.0960	3.520	-.890	4.700
4	4.420	37.500	46.700		.232	6	.140	3.560	-1.440	9.500
5	3.550	42.800	52.100		.223	5.600	.110	3.480	-2.180	18.200
6	4.830	40.100	50.100		.272	6.220	.0900	3.740	-1.690	9.550
7	4.950	38.600	48.100		.248	6.200	.129	3.210	-1.520	8.200
8	5.750	42	52		.338	7.700	.150	5.430	-1.470	9.900
9	4.780	38.500	46.600		.258	7.600	.110	5.170	-1.430	11.100
10	3.760	37.100	47.900		.197	4.320	.180	4.820	-2.450	16
11	4.970	36.900	46.500		.257	6.330	.0950	4.320	-1.440	18.500
12	4.530	36.500	45.500		.232	6.140	.124	4.560	-1.590	11.900
13	4.780	37.300	47.200		.205	4.640	.150	3.770	-1.880	12.100
14	2.340	40.100	46		.130	4.910	.130	2.950	-2.320	18.420
15	4.670	40.400	49.300		.264	7.060	.123	3.430	-1.560	7.970

VARIABLE NO. NAME	TOTAL FREQUENCY	STANDARD MEAN	STANDARD DEVIATION	ST. ERR OF MEAN	COEFF. OF VARIATION	S M A L L E S T VALUE	Z-SCORE	L A R G E S T VALUE	Z-SCORE	RANGE
1 VA	15	4.489	1.184	0.2850	0.24591	2.340	-1.95	7.060	2.33	4.720
2 PACC2	15	38.940	1.944	0.5019	0.04992	36.500	-1.26	42.800	1.99	6.300
3 PCCO2	15	48.000	2.026	0.5231	0.04221	45.500	-1.23	52.100	2.02	6.600
4 VCCO2	15	0.242	0.065	0.0167	0.26746	0.130	-1.73	0.350	2.42	0.220
5 DC	15	6.363	2.014	0.5201	0.31653	4.320	-1.81	12.600	3.10	8.280
6 VD	15	0.125	0.024	0.0061	0.18788	0.090	-1.33	0.180	2.31	0.090
7 frc	15	3.860	0.730	0.1884	0.18904	2.960	-1.23	5.430	2.15	2.470
8 E8	15	-1.735	0.423	0.1091	-0.24364	-2.460	-1.72	-0.890	2.00	1.570
9 T8	15	18.236	2.419	0.6247	0.23636	4.700	-2.29	16.000	2.38	11.300

Table 2.1

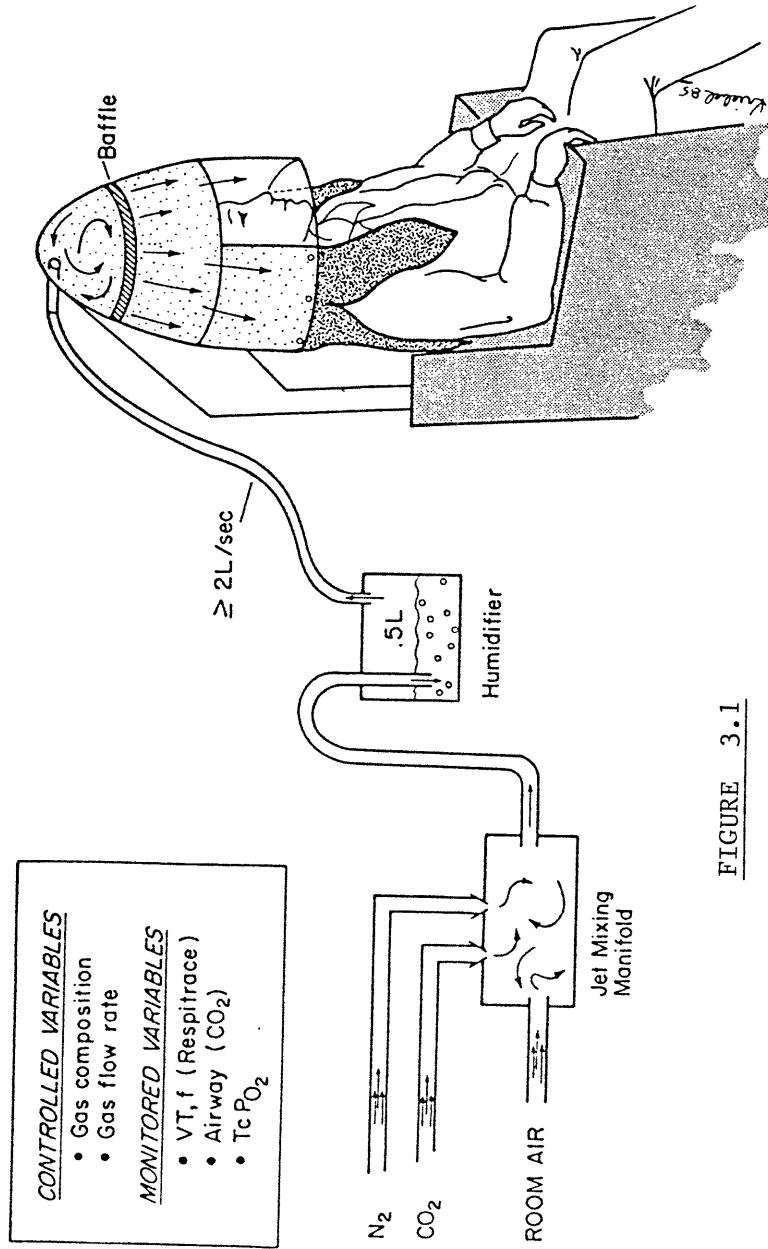


FIGURE 3.1

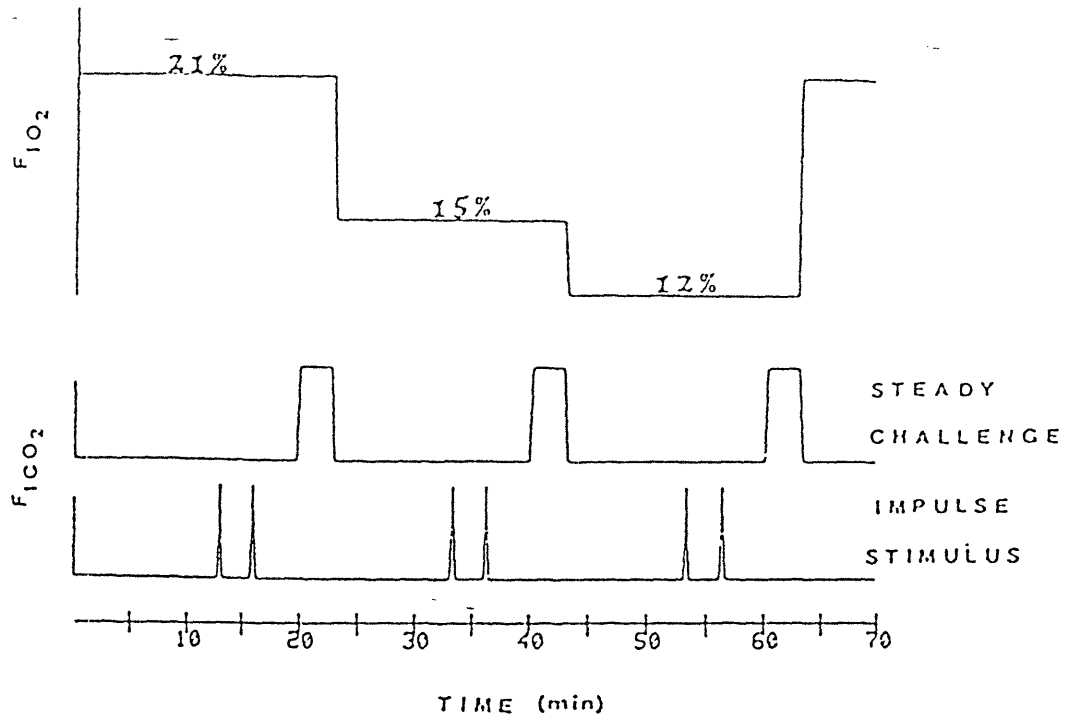


FIGURE 3.2

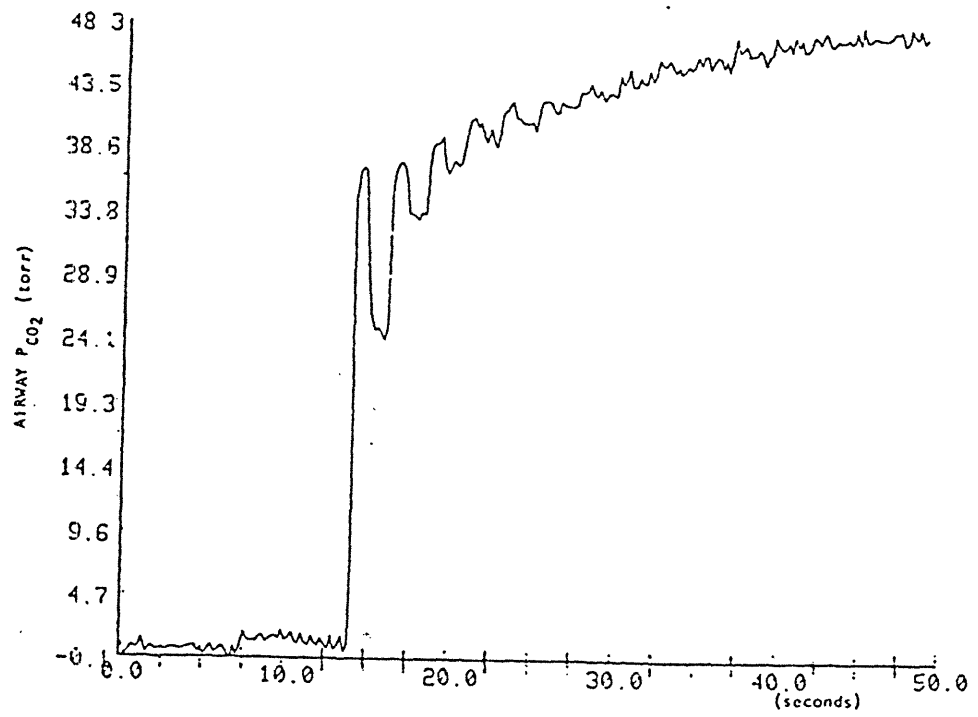


FIGURE 3.3

TRANSIENT RESPONSE.

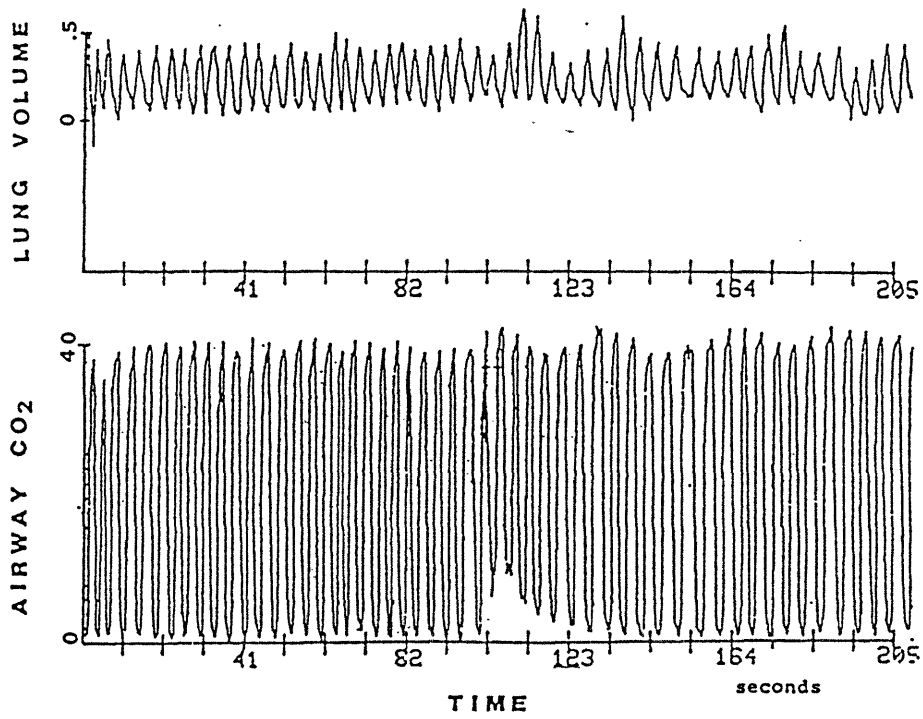


FIGURE 3.4

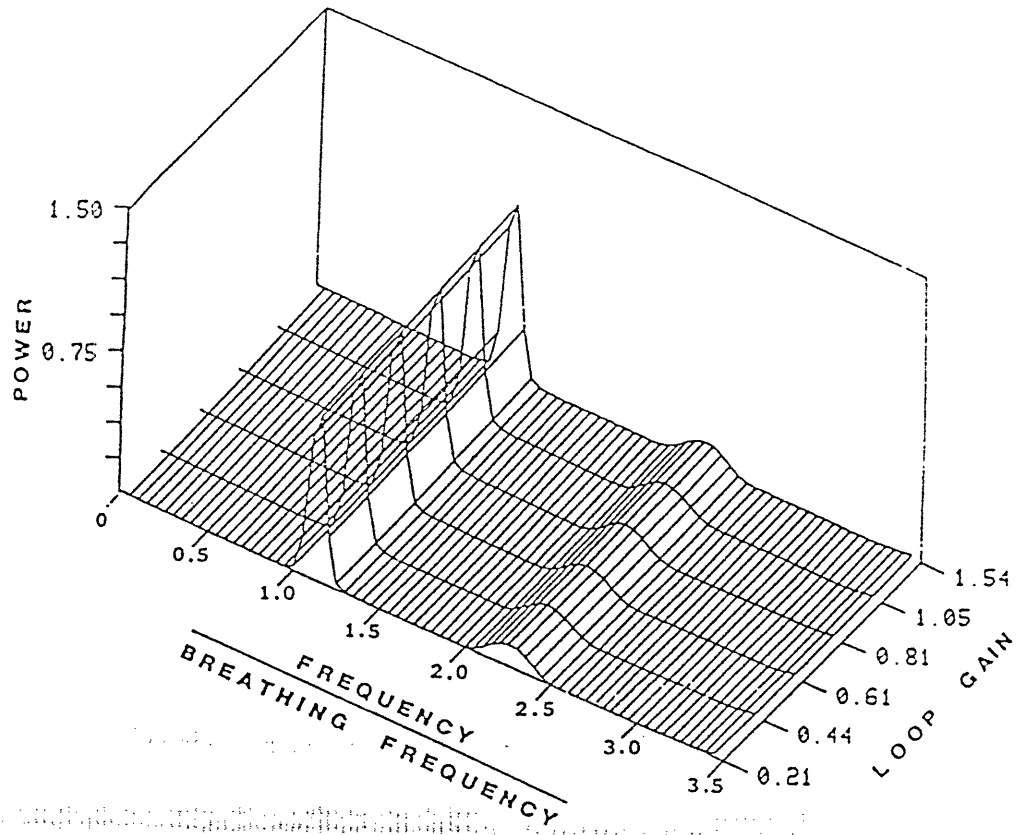


FIGURE 3.5

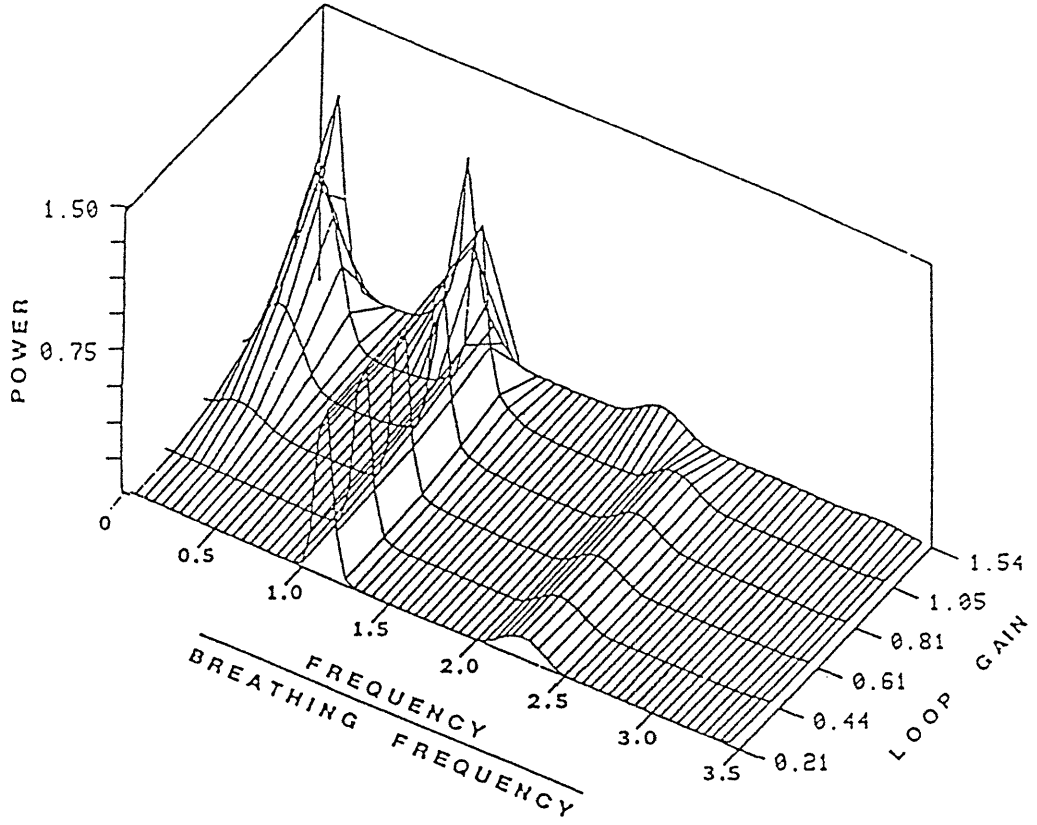


FIGURE 3.6

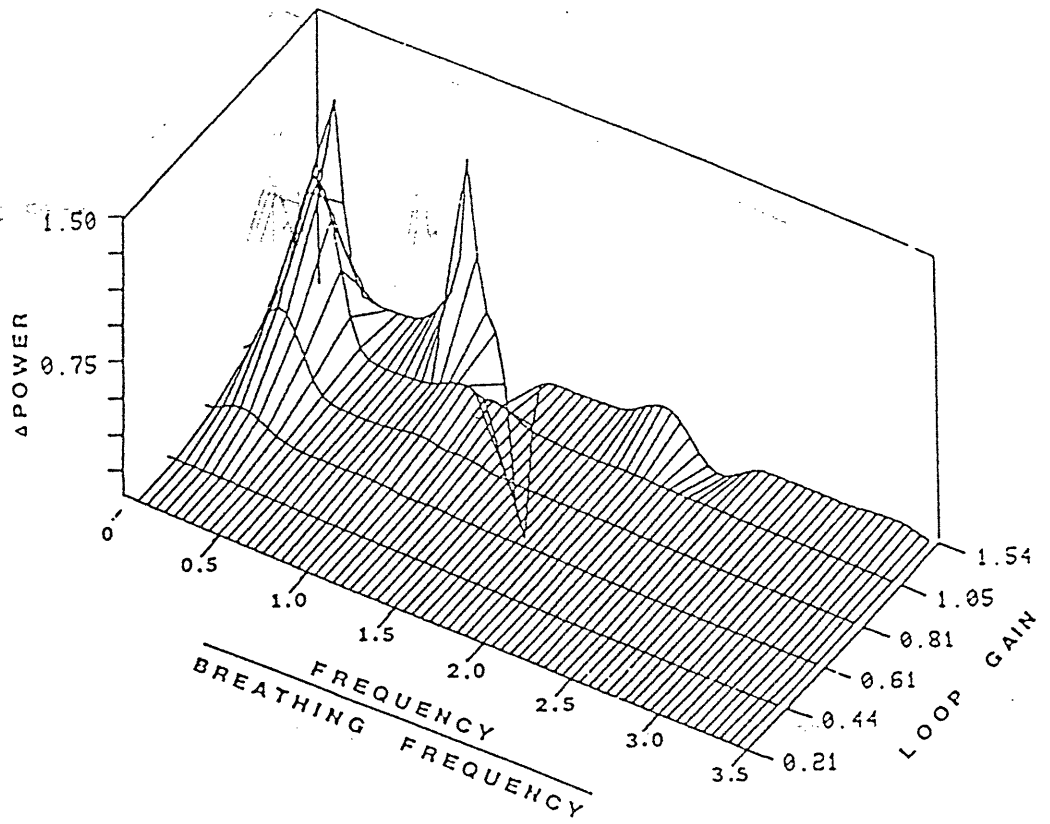
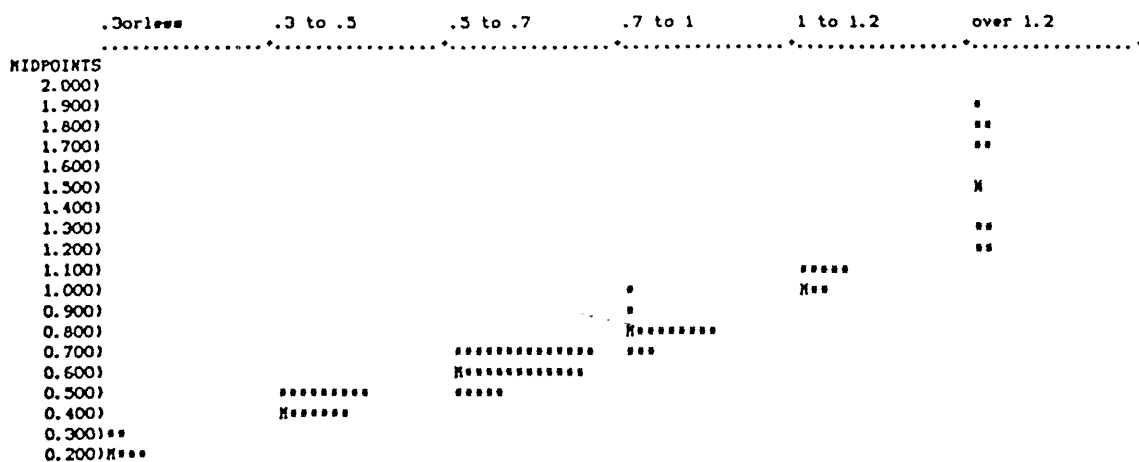


FIGURE 3.7



GROUP MEANS ARE DENOTED BY M'S IF THEY COINCIDE WITH *'S, M'S OTHERWISE

MEAN	0.212	0.437	0.612	0.809	1.049	1.540
STD. DEV.	0.044	0.048	0.053	0.079	0.036	0.301
R. E. S. D.	0.048	0.059	0.059	0.075	0.029	0.363
S. E. M.	0.018	0.012	0.009	0.021	0.013	0.100
MAXIMUM	0.260	0.490	0.690	1.000	1.130	1.910
MINIMUM	0.150	0.370	0.530	0.710	1.020	1.210
SAMPLE SIZE	6	16	32	14	8	9

FIGURE 3.8

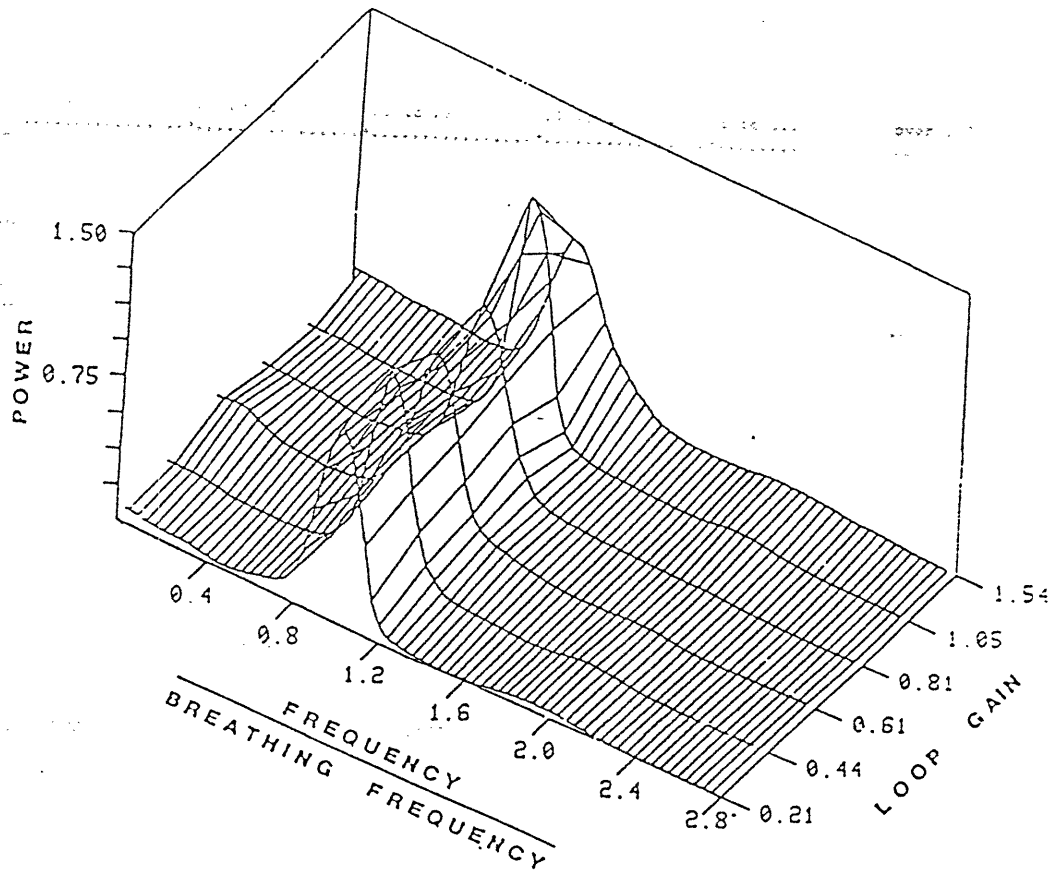


FIGURE 3.9

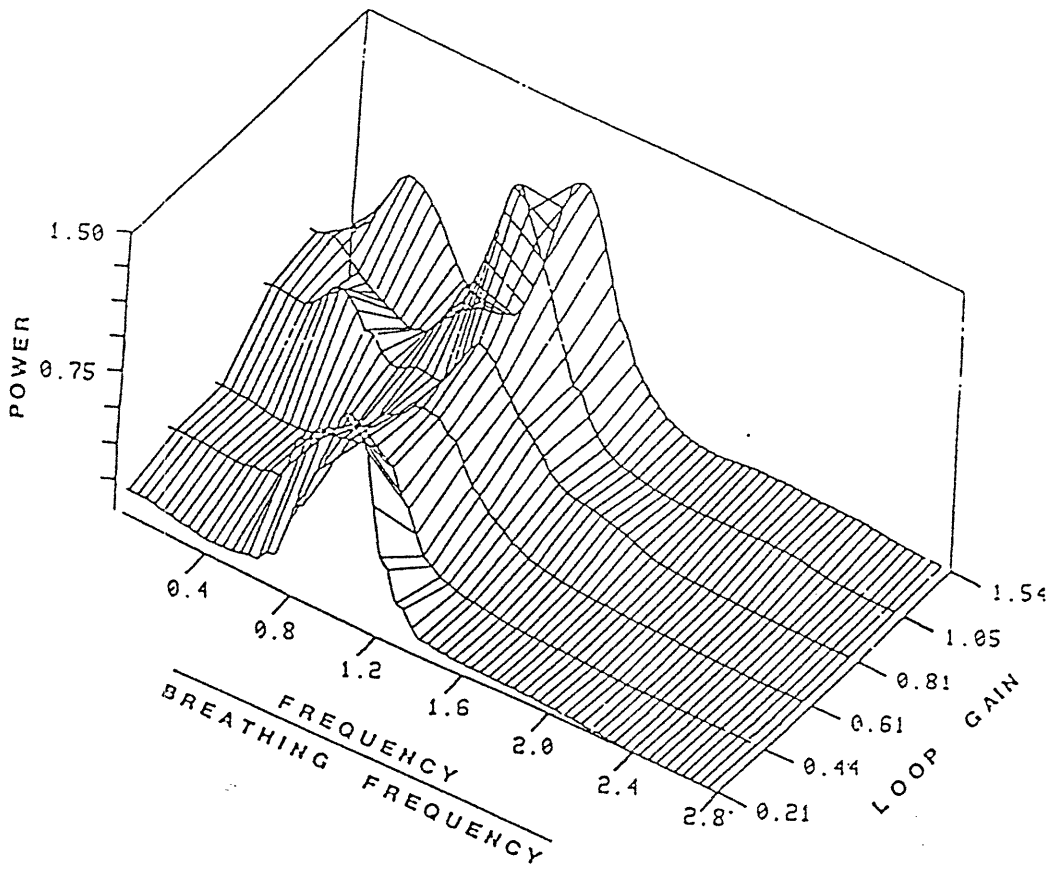


FIGURE 3.10

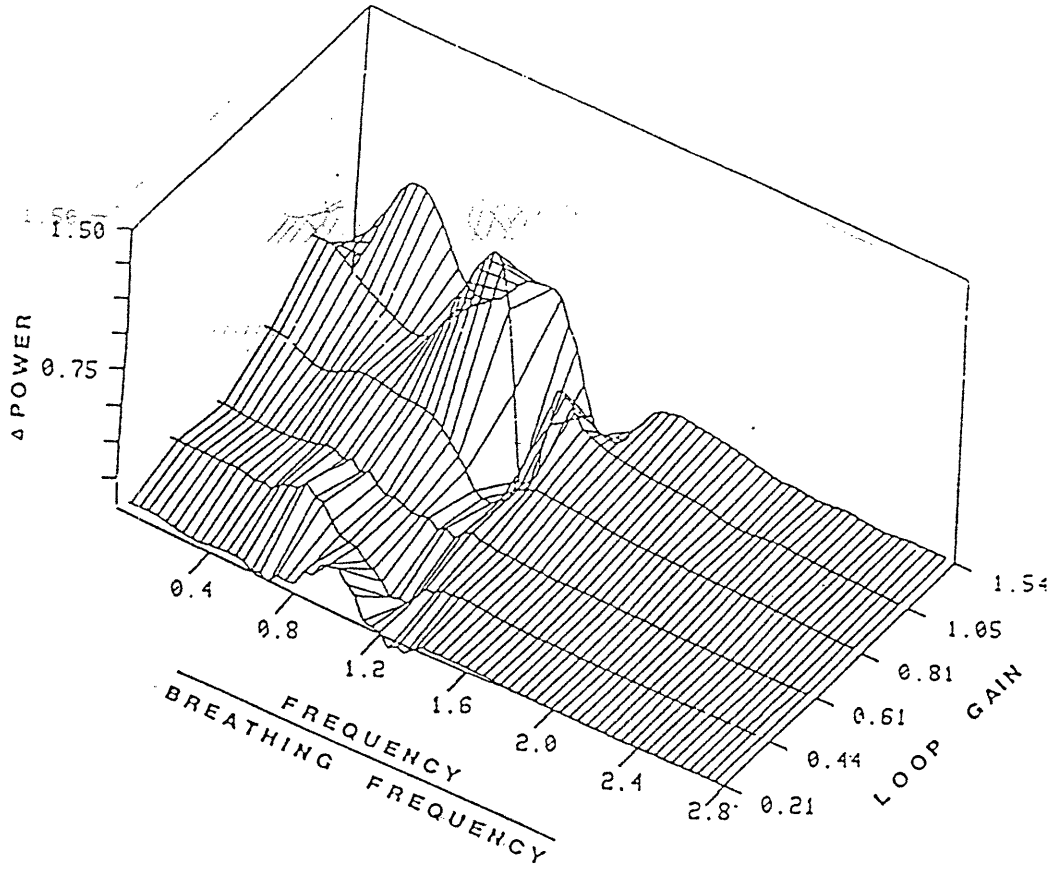


FIGURE 3.11

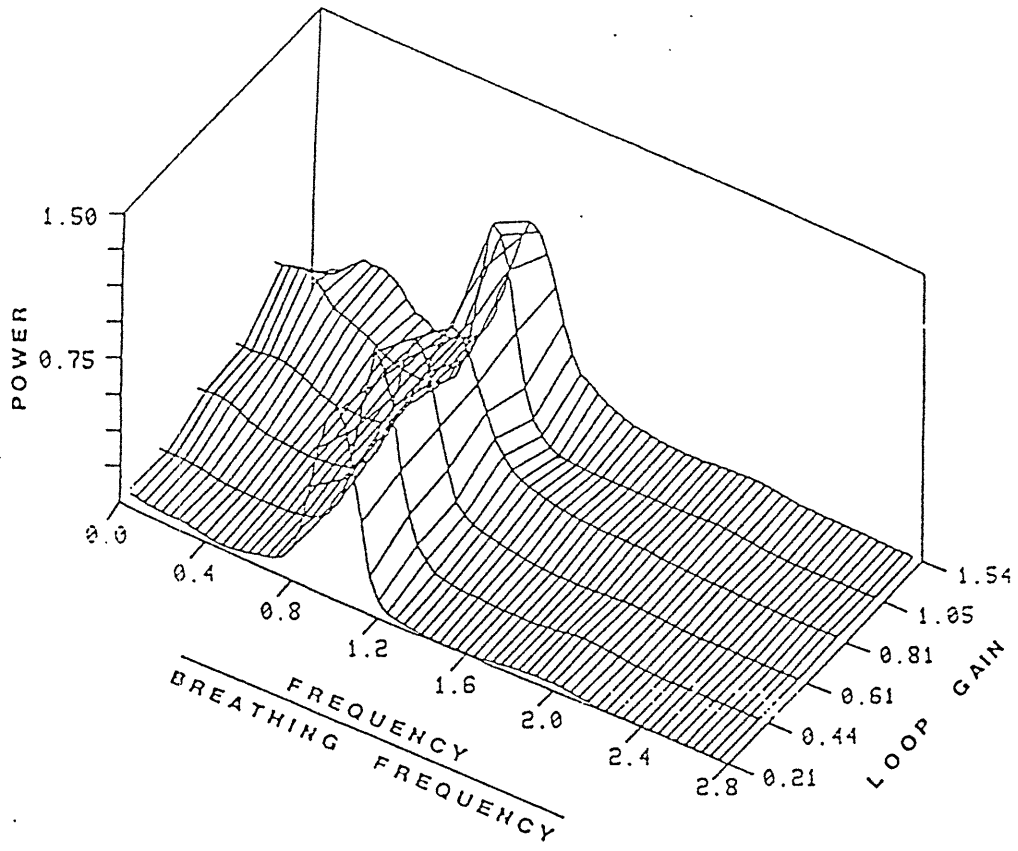


FIGURE 3.12

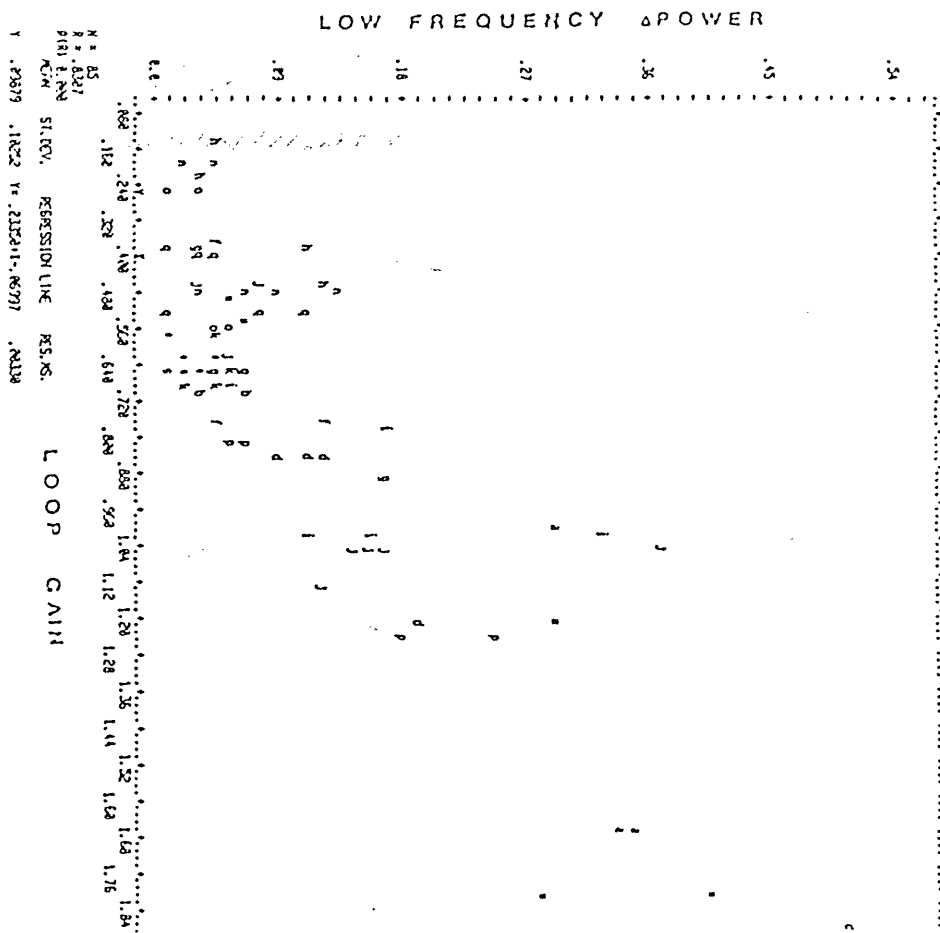


FIGURE 3.13

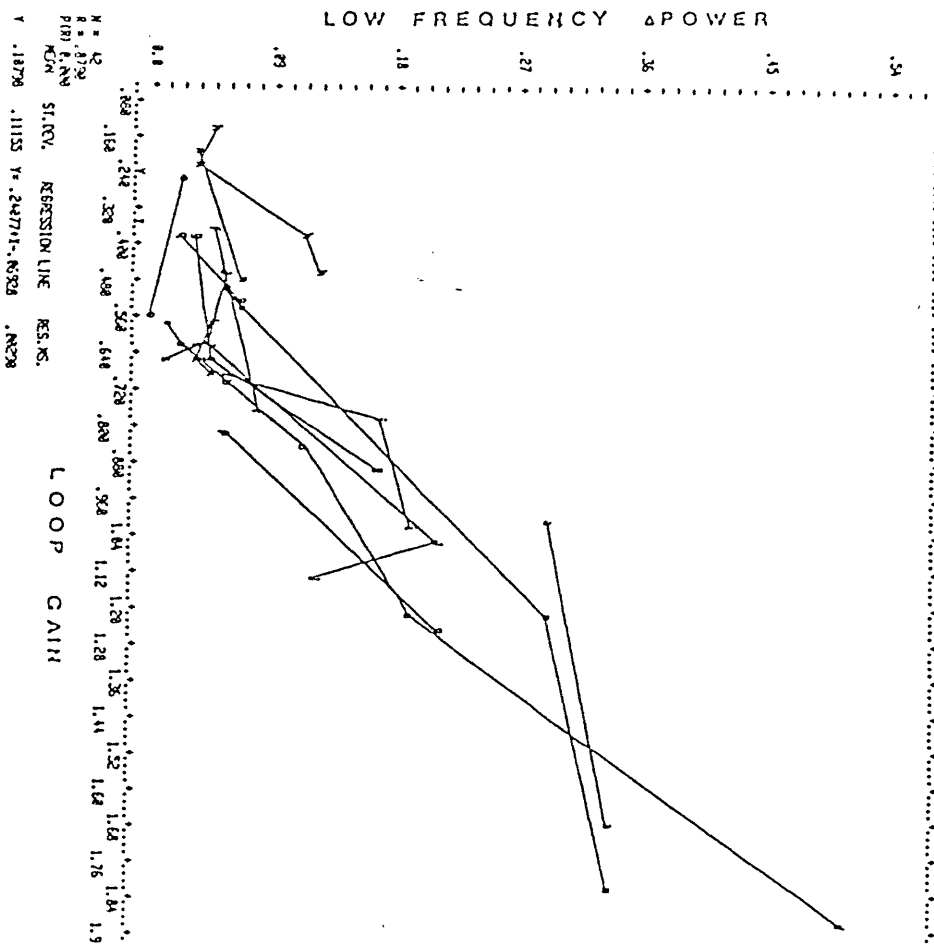


FIGURE 3.14

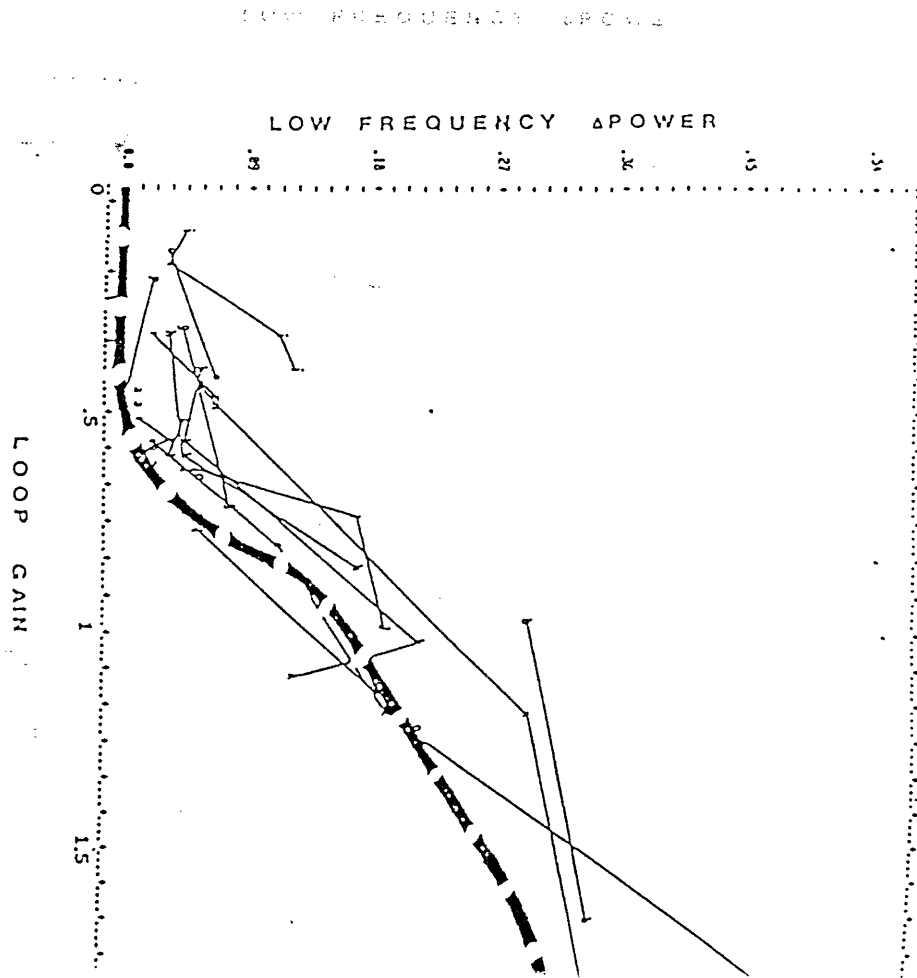


FIGURE 3.15

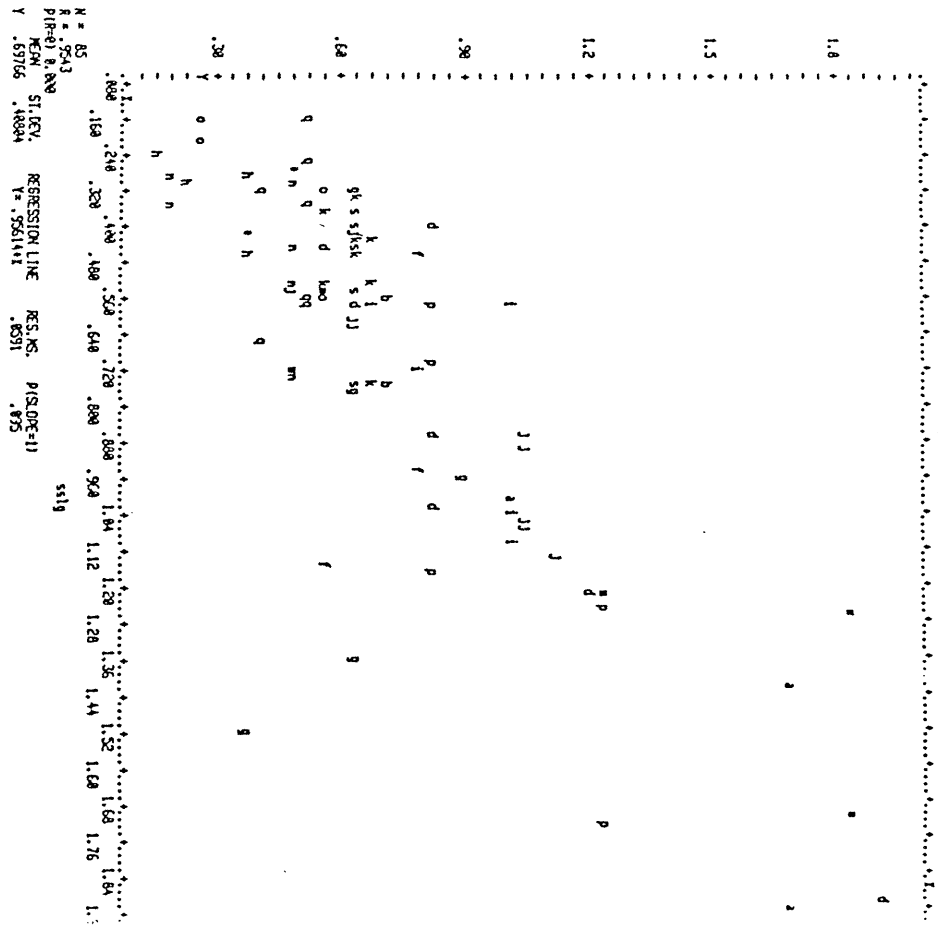


FIGURE 3.16

APPENDIX 1

COMPUTATION OF POWER DENSITY SPECTRA

Resolution of the technique:

The power spectral density (PSD) functions described in this study have been computed using fast Fourier transform (FFT) techniques. This transformation converts a set of N consecutive time domain samples to a set of N/2 frequency domain samples such that;

$$T = NI$$

where,

N = number of samples

I = inter-sample interval

T = total duration of sampling

and

$$FI = \frac{1}{T}$$
$$FMAX = \frac{1}{2T}$$

FI = frequency spacing

FMAX = maximum frequency

The resolution in the frequency domain is directly proportional to the temporal duration of the waveform analyzed. In these studies, each of the epochs analyzed consisted of 512 samples spaced at .2 second intervals. In order to improve the frequency resolution, 512 zeroes have been appended to each of these time series. It is well known that this doubles the density of points in the frequency domain without changing

the PSD estimates at the original frequencies (60). The FFT of each "padded" epoch consisted of 512 complex valued points spaced at .0049 Hz intervals. The raw power spectral density function (or periodogram) was computed as the magnitude of each complex value divided by the frequency spacing (.0049 Hz). Thus, the units of the PSD were magnitude squared per cycle per second.

Estimation Error in the Computed PSD

Because the ventilation waveforms analyzed in this study contain both random and deterministic components, the above technique provides only a statistical estimate of the "true" PSD. If we model the random component of the waveform as uncorrelated Gaussian noise, the mean square error of the raw PSD is unity (60). In other words, the coefficient of variation for each point of the raw PSD waveform is unity. Two common techniques used to reduce this estimation error are; 1) averaging multiple periodograms and 2) smoothing the periodogram.

To use the averaging technique, the periodograms must come from separate time series which may be expected to have identical power spectra. We have employed this technique by defining narrow loop gain ranges, and averaging the normalized spectra from separate transients within each range. This is most appropriate for the control and response spectra, as the perturbation magnitude is not a factor. When averaging M periodograms, the standard error of the estimate decreases to $(1/M)^{.5}$.

We have also employed the smoothing technique to decrease the estimation error associated with each raw PSD. This smoothing was performed

by computing a weighted average of each periodogram value with its M nearest neighbors. We have employed a raised cosine weighting function to average each value with its four nearest neighbors. The bandwidth covered by this averaging is .0245 Hz. Thus, the effective resolution of the PSD is decreased by the smoothing technique. Smoothing over M nearest neighbors decreases the standard error of the PSD estimate to $(1/M)^{.5} = .5$.

The Effect of Spectrum Normalization:

Two separate normalizations have been performed on the smoothed periodograms obtained from the 85 transients analyzed in this study; 1) control, post-stimulus, and response spectra from each transient have been normalized by the area of the carrier peak in the control epoch, and 2) the response spectrum from each transient has been normalized by the perturbation magnitude. We shall assume that the uncertainty in calculating the perturbation magnitude is negligible. This normalization is then equivalent to a simple scaling operation, and the coefficient of variation for the periodogram is unaffected. Normalizing by the area of the control peak does have a statistical effect, however.

If we return to our assumption that the random component of the ventilation waveforms may be modeled as uncorrelated Gaussian noise, the uncertainty associated with each periodogram value is described by a Chi-square distribution with $2M = 8$ degrees of freedom. In performing the normalization, this uncertainty is divided by the area of the control peak. The magnitude of the area, however, is computed from the control PSD, and therefore represents only an estimate of the true area. In fact, the uncertainty associated with this estimate is described by a

Chi-square distribution with $2MK$ degrees of freedom; where K is the number of PSD points spanned by the control peak. Thus the uncertainty in each normalized PSD value is given by the ratio of 2 Chi-square distributed errors. This ratio is given by the F distribution which is characterized by a numerator degrees of freedom ($= 2M$) and a denominator degrees of freedom ($= 2MK$). In this case, $2M = 8$ and $2MK$ is typically 160. The effective standard error for these values is approximately .75. This inherent uncertainty provides strong motivation for averaging the spectra of transients obtained at similar loop gains, as described above.

APPENDIX 2

The goal of this section is to demonstrate the relative stability of the "normal" operating point, as defined by typical population values. In addition, the effect of congestive heart failure (CHF) is simulated. No attempt is made to determine if the model can quantitatively account for all conditions known to induce CSR in humans.

Table A2.1 lists the physiologic parameter "norms" we have used to characterize the awake, resting adult at sea-level. These values result in the following;

$$B = -74 \text{ torr liter}^{-1} \text{ s}^{-1}$$

$$T_0 = 6.4 \text{ s}$$

$$f_c = .05 \text{ Hz}$$

$$A|B(f_c)| = .54$$

Thus we would predict that the "normal operating point" of the control system is indeed stable, with a relative gain margin of approximately 2. It is interesting to note the excellent agreement with the observations of Cherniack et. al. (64) who found that doubling the loop gain induced sustained oscillations in approximately one third of their experimental animals.

The relative stability of this normal operating point is graphically illustrated in figure A2.1. This Nyquist diagram is a phase-plane plot describing the complex loop gain with frequency (or period) used as a parameter. At any given frequency, $|LG(f)|$ is represented as the magnitude of a vector and $\angle LG(f)$ is given by the angle (ϕ) of the same vector. The "unit circle" provides the scale for $|LG(f)|$ and the cartesian

axes provide the scale for $\langle LG(f) \rangle$. The solid curve is the trace made by the tip of the vector as the frequency is altered.

The stability criteria can be conveniently translated to the Nyquist plot. If and only if the vector tip crosses the $\phi = 180^\circ$ axis inside the unit circle, the system is stable. In addition, the Nyquist plot provides a geometric illustration of the relative margin of stability, or gain margin. This gain margin is represented by the distance of the 180° axis crossing from the unit circle. Thus by illustrating the curves associated with different operating points we may conveniently compare their relative stabilities. For example, if we simulate the experiment of Cherniack et. al. (64) and double the controller gain, the effect is shown in figure A2.2. We see clearly that this new operating point just meets the criterion for sustained oscillations. Also note that the period at which the oscillations occur is 20.5s. This agrees well with observations of CSR in healthy adults (37).

The result of simulating congestive heart failure (CHF) is illustrated in figure A2.3. We have assumed that the only significant change in equilibrium conditions found in CHF may be modeled by decreasing the cardiac output and increasing the circulation delay, each by a factor of 3 (3,65). These changes have the following effect;

$$P_{vCO_2} = 58.6 \text{ torr}$$

$$B = -175.7 \text{ torr liter}^{-1} \text{ s}^{-1}$$

$$T_0 = 14.2 \text{ s}$$

$$T_C = 18.6 \text{ s}$$

$$f_c = .018 \text{ Hz (period} = 55.2 \text{ s)}$$

$$|LG(f_c)| = 1.53$$

The model is unstable with this operating point, and oscillates with a period of 55.2 seconds. This period is in good agreement with CSR observed in CHF (3,65,1), including the classic observations of J. A. Cheyne (2) who described oscillations which "occupied about a minute". Two factors act to destabilize the CHF operating point; 1) the increase in B which results directly from the decreased \dot{Q}_C , and 2) the decrease in f_c which results from increases in both T_C and T_0 . Although a ceteris parabis increase in T_0 would tend to decrease $|B(f_c)|$ and stabilize the system, the decrease in f_c accompanying the increased T_C counterbalances this effect in the CHF simulation.

The foregoing analysis demonstrates several points. Despite the simplicity of the present model, it agrees admirably with our expectations based on both experimental observations, and previous modeling work. The model is seen to produce oscillations of appropriate frequency when either increased controller gain or CHF is simulated.

At this point, we must re-emphasize the significance of the minimal modeling approach. The goal of this approach is to clearly define one or more measures of model performance, and a set of conditions under which this performance should be tested. The value of a model is then measured not solely by its performance but also by its complexity. The optimal condition would be to discover the simplest model which performs as well as all more complicated models. We have focussed on two metrics of model performance; 1) the ability of a model to accurately predict the relative stability of any equilibrium operating point, and 2) its ability to predict oscillations of the correct frequency. It should be noted that these performance measures are consistent with

those employed in previous modeling work (15,9,14,10,12,16,13).

In order to minimize the complexity of this model with regard to previous models, we have made certain sacrifices regarding the conditions under which the model behavior may validly be considered. First, the model describes only the local stability about an equilibrium operating point. It cannot simulate the effects of non-local perturbations or transitions from one equilibrium to another. These were the two conditions which allowed us to linearize the hyperbolic function describing the physiologic controlled system. A third limitation is that we have not explicitly included the effect of hypoxemia in our model. It is known that hypoxemia has the effect of increasing the controller gain, A . However, as we are only modeling the behavior about equilibria, we can account for steady-state changes in arterial oxygen tension as equivalent changes in the equilibrium controller gain. For example, employing the formulation of Cherniack et. al. (16) for the effect of hypoxia on A , we would predict a gain increase of 100% to cause oscillations if P_{ICO_2} were reduced to 116 torr. This prediction is also supported by the controlled observations of Waggener et. al. (37). Within these constraints, the benefits of minimal modeling are substantial.

As previously noted, an immediate benefit to linearizing the model is that relationships between variables may be stated explicitly and analytically. Khoo et. al. (15) recently published the first and only linear model of CSR. These authors clearly appreciated the potential benefits of linear modeling. However, while they showed that their

model predicted instability under a variety of conditions known to induce oscillations in some individuals, they made no attempt to follow a true minimal modeling approach.

The Khoo model contains three controllers; one dependent on O_2 , one dependent on CO_2 , and one dependent on O_2 and CO_2 . They also include two separate circulation delays with magnitudes which are functions of the arterial oxygen partial pressure. Finally, in modeling the frequency response of the controlled system, they include the effect of mechanical mixing of the blood within the circulatory system. From the results described here, we see that these complexities may not be necessary in order to accurately characterize the relative stability of the biological control system at important operating points.

As the model of Khoo has been the most successful and thorough in accounting for CSR in humans, we characterized the "normal" operating point of our model using parameter values taken from Khoo (15), where appropriate. The stability of the normal operating points of these two models is compared in figure A2.4. Both operating points are stable. However, the margin of stability for the Khoo model is 600% as opposed to 200% for our model. This quantitative difference motivates the following question; given the normal ranges of the model parameters, are the gain margins of these two models significantly different?

Table A2.2 presents the normal values and ranges for the parameters required to characterize our model. Table A2.3 demonstrates the range of relative stabilities which can be obtained for this model using only "normal" parameter values. The value of $A|B(f_c)|$ spans more than an order of magnitude. Approximately one third of this range is accounted

for by variability in the magnitude of the controller gain, while approximately two thirds is a result of variability in $|B(f_c)|$.

In performing these calculations we do not attempt to rigorously account for the correlations which may occur between parameter values within individuals. Rather, the intent is to evaluate the expected range of normal breathing stability based on model predictions. The conclusion is that the range of relative stabilities spanned by normal parameter ranges encompasses a wide range of breathing behaviors; both stable and unstable.

This finding is certainly not proof that the model structure is inappropriate or inadequate. It is an illustration of two points; 1) if the model accurately predicts human respiratory control, then the cross section of breathing patterns which may be seen in normal resting adults is very broad and will include observations of sustained oscillations; and 2) in order to quantitatively validate the predictive ability of this or any more complex model of respiratory stability, the comparisons must be made in a series of individuals rather than on population norms. This point deserves additional discussion.

It may be argued that despite the fact that the range of normal stabilities may indeed be broad, by looking at "average" parameter values, the average conditions under which oscillations will occur can be predicted. If the predictions are accurate, the model is validated. Several problems exist in this approach. First, as previously noted, there may be no clear consensus regarding the correct "average" parameter values. For example, even for the solubility coefficient of CO_2 in blood, which can be directly measured, the "normal" value employed in different models ranges from .00425 (11,14,59) to .0065(16,15) and .0066

(9).

Second, even knowing the "true" population norms, it may be very difficult to define the "average" conditions under which normal adults may exhibit oscillatory breathing. Good data regarding the value of each parameter under conditions of oscillations may not be available. This fact also raises the issue that there may exist no "normal" individual characterized by a set of population normal parameter values who will exhibit oscillations under a set of average conditions. Thus testing a model on this population basis leaves open at least some question regarding its ability to account for the breathing control of any single individual.

Returning to the comparison between our model and the model of Khoo, it is clear that we cannot claim a quantitative distinction between the two normal operating points. This is not to say that the two models are equivalent; only that they characterize the normal operating point of resting adults equally well. Having demonstrated this equivalence, it is worth noting that the Khoo model requires 18 rather than 6 parameters to characterize an operating point. It is thus associated with an even wider range of normal operation than is our model.

By following a minimal modeling approach we have derived analytic relationships which define the model stability in dimensionless terms and also predict the frequency of unstable oscillations. The behavior of the minimal model when constrained by "population normal" parameter values is in good agreement with both experimental observations of CSR and previous non-minimal models of CSR. The desire to quantitatively

validate the predictions of the minimal model for the relative stability of human respiration provides substantial motivation for the experimental work described in chapter 2.

TABLE A2.1

Parameter	Units	Value
\dot{Q}_C	$l s^{-1}$.10
K_{s1}		.0065
frc	l	3.2
T_C	s	6.1
P_{vCO_2}	torr	46.2
P_{aCO_2}	torr	40
\dot{V}_A^o	$l s^{-1}$.071
A	$l s^{-1} torr^{-1}$.0165
P_B	torr	760
P_W	torr	47

TABLE A2.2

Parameter	Units	Value	Range
\dot{Q}_C	$l s^{-1}$.10	.05 - .15
K_{s1}		.0065	.004 - .007
frc	l	3.2	2 - 5
T_C	s	6.1	4 - 8
P_{vCO_2}	torr	46.2	45 - 52
P_{aCO_2}	torr	40	38 - 42
\dot{V}_A^o	$l s^{-1}$.071	.04 - .10
A	$l s^{-1} torr^{-1}$.0165	.0125 - .03

TABLE A2.3

Minimal "Normal" Loop gain

$$B_0 = \frac{.15(713)(.007)(45)}{(.15(713)(.007) + .10)^2} = -40.11$$

$$T_0 = \frac{5}{.15(713)(.007) + .10} = 5.89s$$

$$T_C = 4s \quad f_c = .077Hz \quad |B(f_c)| = 13.28 \quad A|B(f_c)| = .16$$

Maximal "Normal" Loop Gain

$$B_0 = \frac{.05(.004)(713)(50)}{(.05(.004)(713) + .04)^2} = -213.39$$

$$T_0 = \frac{2}{.05(.004)(713) + .10} = 10.9s$$

$$T_C = 8s \quad f_c = .038Hz \quad |B(f_c)| = 75.77 \quad A|B(f_c)| = 2.27$$

FIGURE CAPTIONS

Figure A2.1: Nyquist diagram representation of the "normal adult" operating point of the linear model. In this plot, both LGM(f) and LPS(f) are plotted using $T = 1/f$ as a parameter. For any oscillation period, these two quantities are represented as a single vector with a Euclidean length of LGM(f) and an angular orientation of LPS(f). The 'unit' circle illustrates the length of a vector with a length of unity, as shown in the figure. The cartesian coordinates provide the scale in degrees for the value of LPS(f). The solid curve is the trace of the vector tip as the period is altered. The labeled asterisks indicate the value of the period seconds. The stability criterion may be stated: if the curve representing an operating point crosses the 180 degree axis inside the unit circle, the operating point is locally stable. Note that the distance from the unit circle at which this axis crossing occurs provides a geometric interpretation of the 'relative' stability of any operating point. This figure indicates that the "normal" operating point is indeed stable, with a gain margin of 200%.

Figure A2.2: Illustrates the effect of doubling the normal controller gain, ceteris parabis. This new operating point just fails to meet the stability criterion, and the model will oscillate at a period of approximately 20 s.

Figure A2.3: Simulated operating point of congestive heart failure. Represents an increased circulation delay and decreased cardiac output, each by a factor of 3. With this operating point, the model is

unstable; oscillating with a period of approximately 56 s.

Figure A2.4: Comparison of the "normal" operating points of our model and the linear model of Khoo et. al. (15). Identical parameter values were used in both models, where appropriate. Both models are stable; the Khoo model being relatively more stable by a factor of 3.

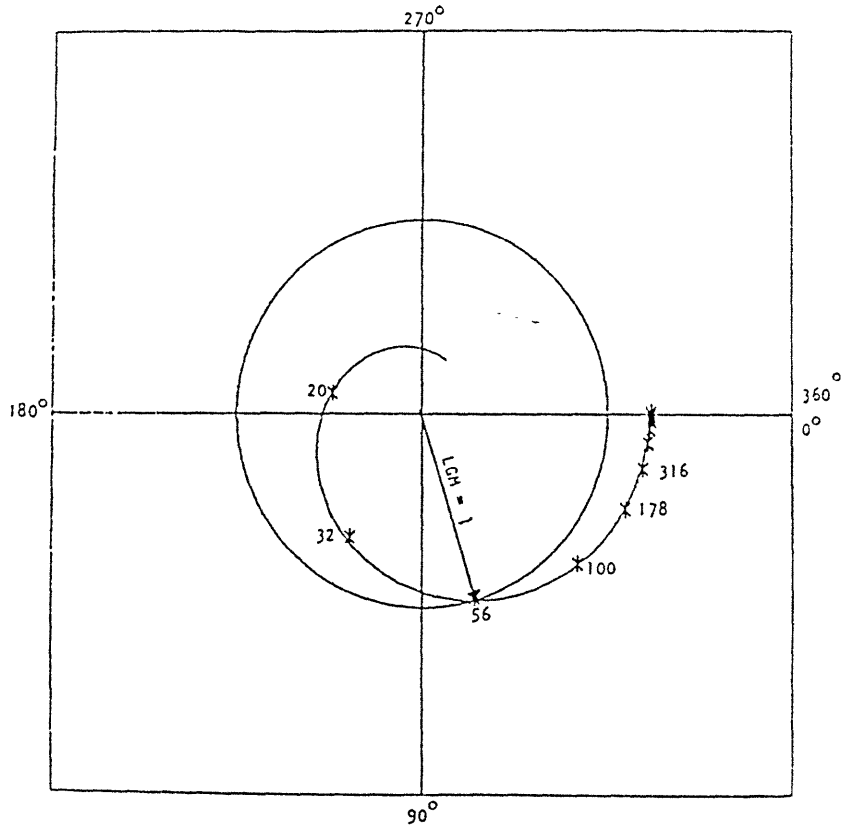


FIGURE A2.1

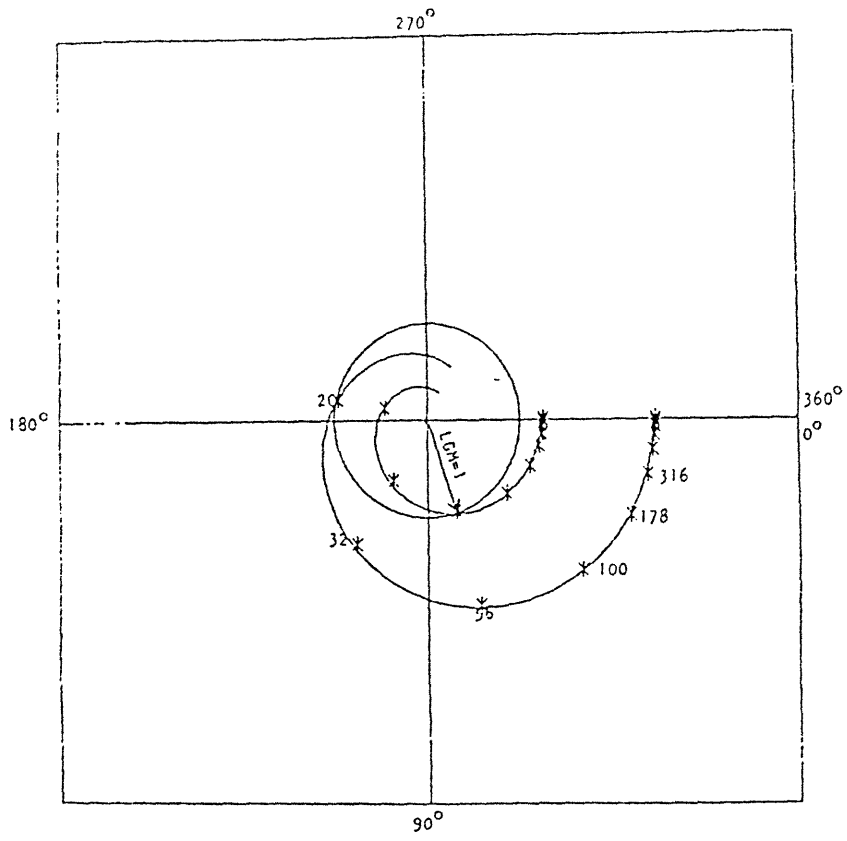


FIGURE A2.2

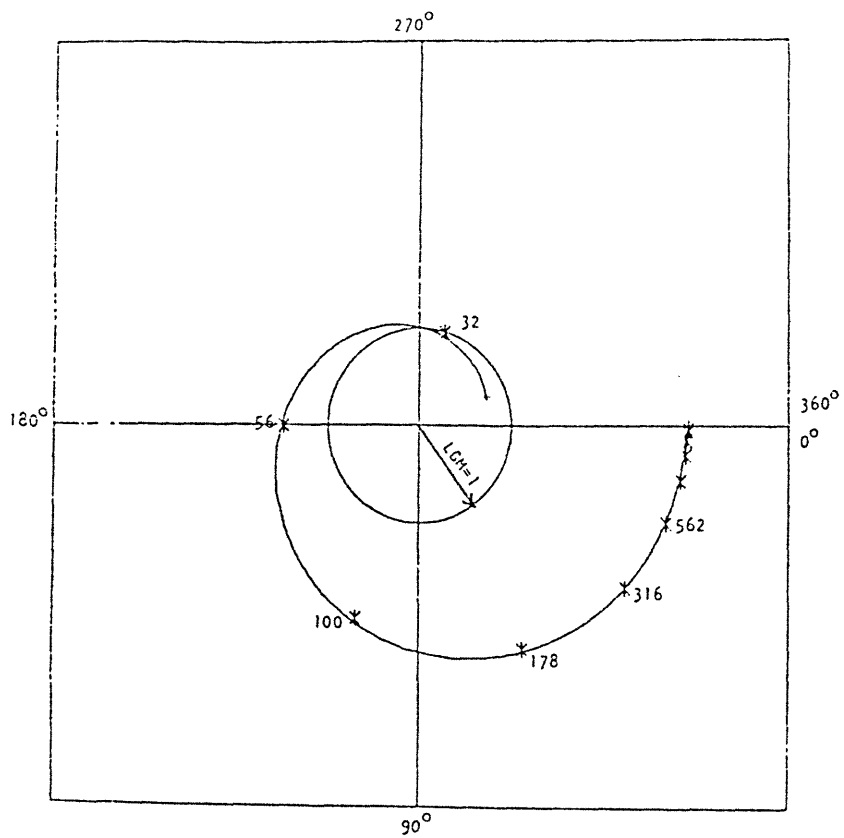


FIGURE A2.3

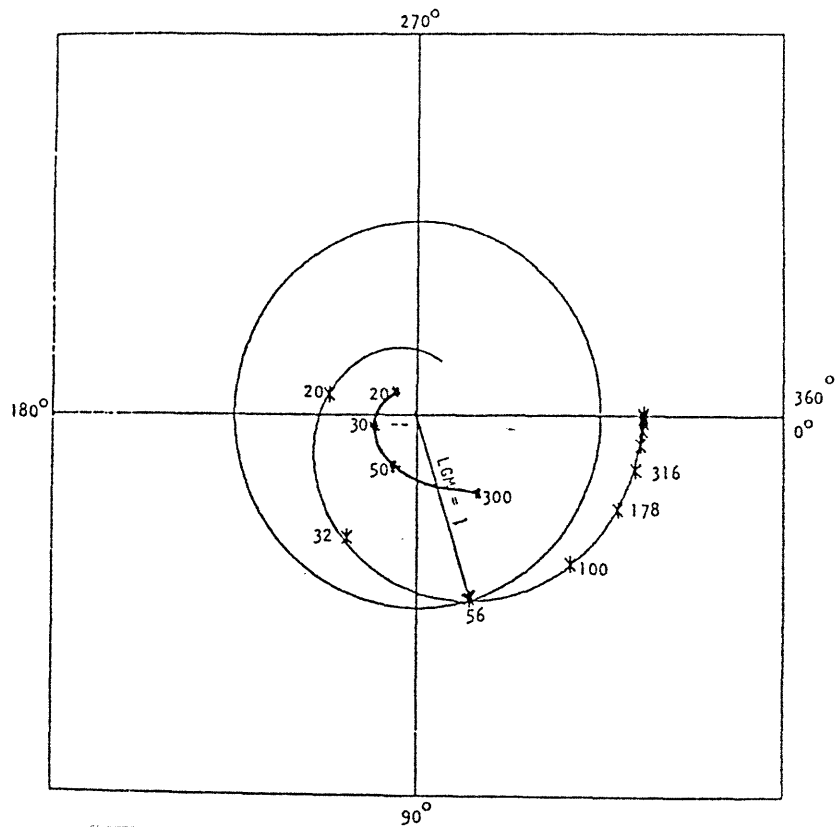


FIGURE A2.4

APPENDIX 3

Describing Function Analysis and the Minimal Model

Describing functions provide a method for the analysis of nonlinear systems that is closely related to the linear-system techniques involving Nyquist, or gain-phase plots. It is possible to use this type of analysis to determine if constant amplitude periodic oscillations (limit cycles) are possible for a given system. We shall use this technique to explore the effects of adding a physiologic saturation nonlinearity to the controller description. The following discussion presents the derivation of the expressions needed to discover if this nonlinearity will allow the minimal control model of breathing to produce limit cycle behavior analogous to Cheyne-Stokes respiration.

Derivation of the Describing Function

A describing function describes the behavior of a nonlinear element for purely sinusoidal excitation. Thus the input signal applied to the nonlinear controller to determine its describing function is;

$$V_I = D \sin(2\pi f_d t) \quad (A3.1)$$

The output of the nonlinear element can be expanded in a Fourier series of the form;

$$V_O = A_1(D, 2\pi f_d) \cos(2\pi f_d t) + B_1(D, 2\pi f_d) \sin(2\pi f_d t) + A_2(D, 2\pi f_d) \cos(2\pi f_d t) + B_2(D, 2\pi f_d) \sin(2\pi f_d t) + \dots + \quad (A3.2)$$

The describing function for the controller is then defined as;

$$A'(D, 2\pi f_d) = \frac{(A_1^2(D, 2\pi f_d) + B_1^2(D, 2\pi f_d))^{.5}}{D} \quad \phi = \frac{A_1(D, 2\pi f_d)}{B_1(D, 2\pi f_d)} \quad (A3.3)$$

The describing function indicates the relative amplitude and phase angle of the fundamental component of the output of a nonlinear element when the element is excited with a sinusoid. In contrast to the case with linear elements, these quantities can be dependent on the amplitude as well as the frequency of the excitation.

The describing function of the controller element

Using the general results developed above, we shall derive the expression used in the text for the gain of the controller element. Once again, the response of this element to sinusoidal excitation is illustrated in figure A3.2. If the amplitude of the input to the saturation is less than \dot{V}_A^o the operation of the controller remains linear with a gain of A. When the input amplitude exceeds \dot{V}_A^o , the effective controller gain is less than A and we must determine its amplitude by solving equation A3.3. In this derivation, we shall employ the notation illustrated in figure A3.2;

$$R = \frac{\dot{V}_A^o}{D}$$

$$a = \sin^{-1}(R)$$

2π = total cycle duration

A = linear controller gain

Thus we have;

$$A_1 = \frac{1}{\pi} \int_0^{\pi+a} AD \sin(2\pi f_d t) \cos(2\pi f_d t) d2\pi f_d t + \frac{1}{\pi} \int_{\pi+a}^{2\pi-a} -A \dot{V}_A^o \cos(2\pi f_d t) d2\pi f_d t$$

$$\begin{aligned}
 & + \frac{1}{\pi} \int_{2\pi-a}^{2\pi} AD \sin(2\pi f_d t) \cos(2\pi f_d t) d2\pi f_d t \\
 & = \frac{AD}{2\pi} ((\sin^2(\pi+a) - \sin^2(0)) + (\sin^2(2\pi) - \sin^2(2\pi-a))) \\
 & \quad - \frac{AV_A^0}{\pi} (\sin(2\pi-a) - \sin(\pi-a)) = 0
 \end{aligned}$$

This result could have been predicted from symmetry arguments, as well.

For B_1 we obtain;

$$\begin{aligned}
 B_1 & = \frac{1}{\pi} \int_{\pi}^{\pi+a} AD \sin^2(2\pi f_d t) d2\pi f_d t + \frac{1}{\pi} \int_{\pi+a}^{2\pi-a} -AV_A^0 \sin(2\pi f_d t) d2\pi f_d t \\
 & \quad + \frac{1}{\pi} \int_{2\pi-a}^{2\pi} AD \sin^2(2\pi f_d t) d2\pi f_d t \\
 & = \frac{AD}{2\pi} (\pi+a - \sin(\pi+a)\cos(\pi+a) - \sin(0)\cos(0) - 0) \\
 & \quad + \frac{AD}{2\pi} (2\pi - \sin(2\pi)\cos(2\pi) - 2\pi+a - \sin(2\pi-a)\cos(2\pi-a)) \\
 & \quad + \frac{AD}{\pi} (\sin(2\pi-a) - \sin(\pi+a))
 \end{aligned}$$

Which reduces to;

$$B_1 = \frac{AD}{\pi} (\sin^{-1}R + R(1-R^2)^{.5} + \frac{\pi}{2})$$

Which gives;

$$A' = \frac{A}{\pi} (\sin^{-1}R + R(1-R^2)^{.5} + \frac{\pi}{2})$$

This is the expression which has been used in the text. It should be noted that due to the non-symmetric nature of the nonlinearity employed, the controller output will have a net increase in its mean output during limit cycle behavior. The effect of this phenomenon on the controlled system is to drive the mean arterial P_{CO_2} to a lower value. The lower

mean P_{CO_2} will in effect cause the controller to clip an even smaller sine wave. Thus, the "effective" gain expression calculated above may be a relative overestimate. However, even when the loop gain is tripled, eliciting the strong oscillations shown in figure A3.3c, the value of R obtained by solving equation 1.25 is only 8% higher than the value observed in simulation (.25 vs .23). Due to the non-linear relationship between the apneic fraction and R , the error in this prediction is even smaller (2%; .42 vs .41). Thus the analytic relationships provided by describing function analysis are indeed an accurate and valuable means of characterizing the model behavior.

One final point is illustrated by the above comparison between the predictions of equations 1.25 and 1.26 and the simulation behavior of the model. Remember that the describing function technique is based on obtaining the effective gain for the controller when it is excited by a pure sinusoid. The close correlation between describing function predictions and simulation results indicate that the P_{aCO_2} is close to sinusoidal. This may be seen visually by inspecting the $P_{aCO_2}(t)$ waveform in figure A3.3.

FIGURE CAPTIONS

Figure A3.1: Input-output relationship of the controller containing a saturation nonlinearity. This saturation corresponds to the physical constraint that alveolar ventilation must be a non-negative quantity. The breakpoint occurs at an arterial P_{CO_2} equal to the setpoint value for the controller. The equilibrium operating point is indicated by $(\dot{V}_{A,P}^o, P^o_{aCO_2})$.

Figure A3.2: Illustrates the sinusoidal method of the testing the operation of the non-linear controller. When the arterial drive to the controller would command a negative ventilation, the saturation clamps the output at zero. Upper sinusoid is the excitation for the nonlinearity, the lower curve is the output.

Figure A3.3: a) Illustrate the genesis of a constant amplitude oscillation. This oscillation is created by suddenly doubling the normal loop gain. Note that the amplitude of the oscillation does not stabilize until the controller output includes periodic apnea, and is thus operating in its nonlinear range. b) and c) illustrate the effect of progressively increasing the loop gain.

constant that directly proportional to the partial pressure of

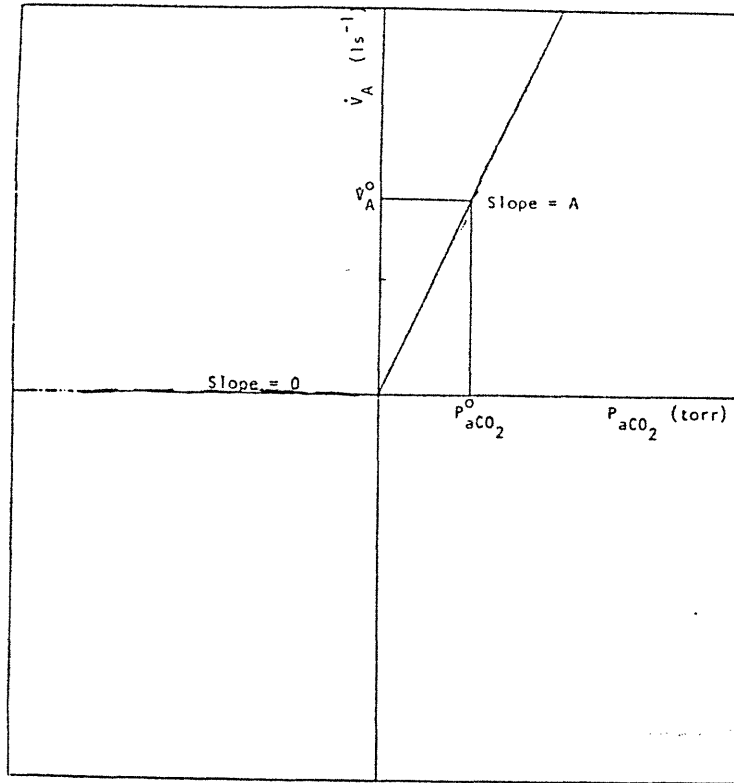


FIGURE A3.1

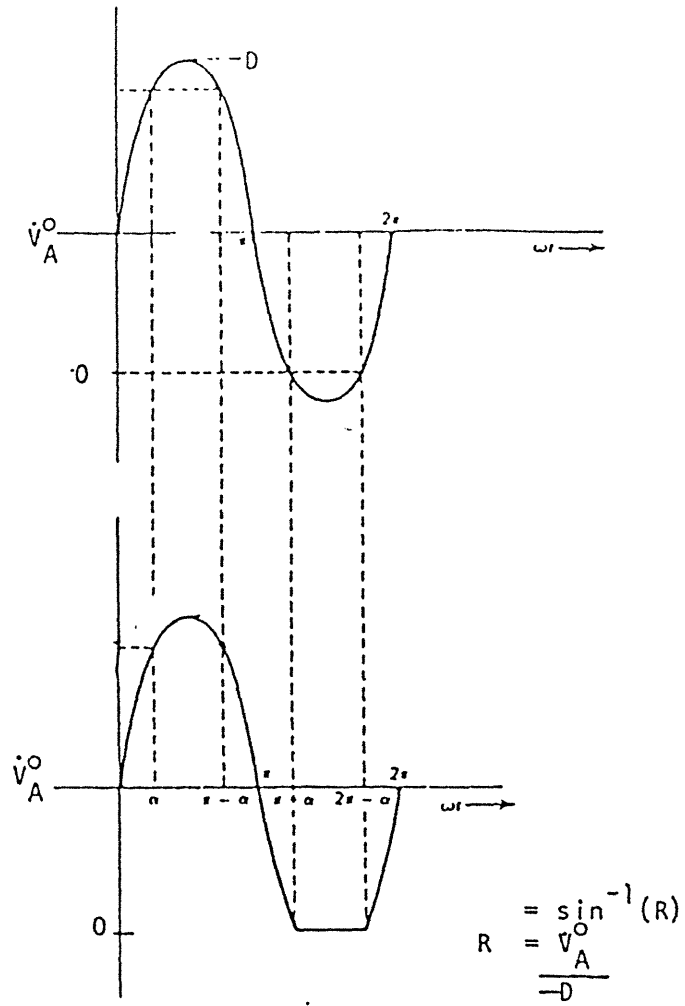


FIGURE A3.2

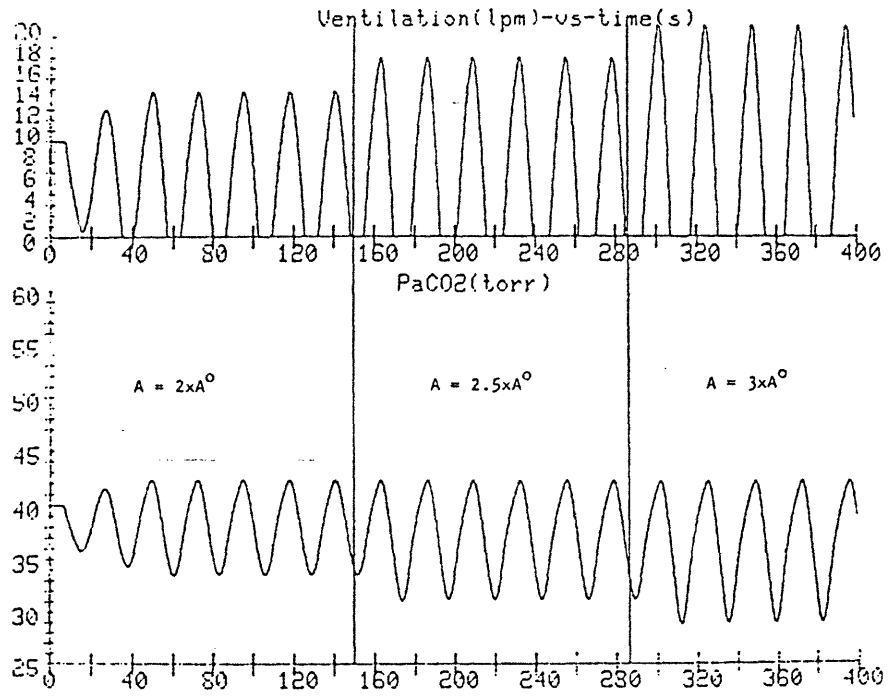


FIGURE A3.4

References

1. A. R. Dowell, C. E. Buckley, R. Cohen, R. E. Whalen, and H. O. Sieker, "Cheyne-Stokes Respiration: A Review of Clinical Manifestations and Critique of Physiological Mechanisms," Arch. Intern. Med., vol. 127, pp. 712-726, April 1971.
2. J. A. Cheyne, "A case of apoplexy in which the fleshy part of the heart was converted into fat," Dublin Hosp. Rep., vol. 2, pp. 216-223, 1818.
3. H. Brown and F. Plum, "The Neurologic Basis of Cheyne-Stokes Respiration," Am. J. Med., vol. 30, pp. 849-860, 1961.
4. M. Marckwald, The Movements of Respiration and Their Innervation in the Rabbit. T. A. Haig (trans), Blackie and Son, London, 1888.
5. W. B. Youmans and R. T. Schopp, "Cheyne-Stokes Breathing after Denervation of Carotid and Aortic Chemoreceptors and Sino-Aortic Pressureceptors," Proc. Soc. Exptl. Biol. Med., vol. 95, pp. 100-101, 1957.
6. T. Bullock, "The origins of patterned nervous discharge," Behavior, vol. 17, pp. 48-59, 1961.
7. G. Preiss, S. Iscoe, and C. Polosa, "Analysis of a periodic breathing pattern associated with Mayer waves," Am. J. Physiol., vol. 228, pp. 768-774, 1975.
8. G. Preiss, F. Kirchner, and C. Polosa, "Patterning of Sympathetic Preganglionic Neuron Firing by the Central Respiratory Drive,"

Brain Res., vol. 87, pp. 363-374, 1975.

9. J. D. Horgan and D. L. Lange, "Analog Computer Studies of Periodic Breathing.," IRE Trans. on Biomed. Elec., pp. 221-228, 1962.
10. J. D. Horgan and R. L. Lange, "Digital Computer Simulation of Respiratory Response to Cerebrospinal Fluid PCO₂ in the Cat," Biophysical Journal, vol. 5, pp. 935-945, 1965.
11. F. S. Grodins and G. James, "Mathematical Models of Respiratory Regulation," Annals New York Academy of Sciences, pp. 852-868, 1965.
12. F. S. Grodins, J. Buell, and A. Bart, A Mathematical Analysis and Digital Simulation of the Respiratory Control System., J. Appl. Physiol., p. 22, 260-276, 1967.
13. H. T. Milhorn, R. Benton, R. Ross, and A. C. Guyton, "A Mathematical Model of the Human Respiratory Control System," Biophysical Journal, vol. 5, pp. 27-46, 1965.
14. H. Milhorn and A. C. Guyton, "An Analog Computer Analysis of Cheyne-Stokes Breathing.," J. Appl. Physiol., vol. 20, pp. 328-333, 1965.
15. M. C. Khoo, R. E. Kronauer, K. P. Strohl, and A. S. Slutsky, "Factors inducing periodic breathing in humans: a general model," J. Appl. Physiol.: Respirat. Environ. Exercise Physiol., vol. 53, pp. 644-659, 1982.
16. G. S. Longobardo, N. S. Cherniack, and A. P. Fishman, "Cheyne-

- Stokes Breathing Produced By a Model of the Human Respiratory System," J. Appl. Physiol., vol. 21, pp. 1839-1846, 1966.
17. M. K. S. Hathorn, "Analysis of the Rhythm of Infantile Breathing.," Br. Med. Bull., vol. 31, pp. 8-12, 1975.
 18. S. T. Nugent and J. P. Finley, "Spectral Analysis of Periodic and Normal Breathing in Infants," IEEE Trans. on Biomed. Eng., vol. BME-30, pp. 672-675, 1983.
 19. S. Lahiri, K. Maret, and M. G. Sherpa, "Dependence of High Altitude Sleep Apnea on Ventilatory Sensitivity to Hypoxia," Respiration Physiology, vol. 52, pp. 281-301, 1983.
 20. I. P. Priban, "An Analysis of Some Short-Term Patterns of Breathing in Man at Rest.," J. Physiol., vol. 166, pp. 425-434, 1963.
 21. C. Lenfant, "Time-Dependent Variations in Pulmonary Gas Exchange in Normal Man at Rest.," J. Appl. Physiol., vol. 22, pp. 675-684, 1967.
 22. L. Goodman, "Oscillatory Behavior of Ventilation in Resting Man.," IEEE Trans. Biomed. Eng., vol. BME-11, pp. 82-93, 1964.
 23. P. J. Brusil, T. B. Waggner, R. E. Kronauer, and P. Gulesian, "Methods for Identifying Respiratory Oscillations Disclose Altitude Effects.," J. Appl. Physiol., vol. 48, pp. 545-556, 1980.
 24. M. K. S. Hathorn, "The Rate and Depth of Breathing in New-Born Infants in Different Sleep States.," J. Physiol., vol. 243, pp. 101-113, 1974.

25. R. N. Bergman, C. R. Brown, and C. Cobelli, "The Minimal Model Approach to Quantification of Factors Controlling Glucose Disposal in Man," in Carbohydrate Metabolism, ed. C. Cobelli and R. Ber, pp. 269-296, J. Wiley and Sons Ltd., 1981.
26. M. Minorsky, Introduction to Nonlinear Mechanics, Edwards, Ann Arbor, 1947.
27. R. S. Fitzgerald, J. Tracz, R. Penman, and J. F. Perkins, "Ventilatory Response to Transient Perfusion of Carotid Chemoreceptors.," Am. J. Physiol., vol. 205, pp. 1305-1313, 1964.
28. R. E. Dutton, W. A. Hodson, D. G. Davies, and V. Chernick, "Ventilatory Adaptation to a Step Change in PCO₂ at the Carotid Bodies.," J. Appl. Physiol., vol. 23, pp. 195-202, 1967.
29. R. E. Dutton, W. A. Hodson, D. G. Davies, and A. Fenner, "Effect of the Rate of Rise of Carotid Body PCO₂ on the Time Course of Ventilation.," Resp. Physiol., vol. 3, pp. 367-379, 1967.
30. R. E. Dutton, R. S. Fitzgerald, and N. Gross, "Ventilatory Response to Square-Wave Forcing of Carbon Dioxide at the Carotid Bodies.," Resp. Physiol., vol. 4, pp. 101-108, 1968.
31. G. D. Swanson and J. W. Belleville, "Hypoxic-Hypercapnic Interaction in Human Respiratory Control," J. Appl. Physiol., vol. 36, pp. 480-487, 1974.
32. J. W. Belleville, B. J. Whipp, R. D. Kaufman, G. D. Swanson, K. A. Aqleh, and D. M. Wilberg, "Central and Peripheral Chemoreflex Loop Gain in Normal and Carotid Body Resected Subjects.," J. Appl.

- Physiol., vol. 46, pp. 843-853, 1979.
33. D. J. C. Cunningham and P. A. Robbins, "The Pattern of Breathing in Man in Response to Sine Waves of Alveolar Carbon Dioxide and Hypoxia," J. Physiol., vol. 350, pp. 475-486, 1984.
 34. P. A. Robbins, "The Ventilatory Response of the Human Respiratory System to Sine Waves of Alveolar Carbon Dioxide and Hypoxia," J. Physiol., vol. 350, pp. 461-474, 1984.
 35. C. G. Douglas and J. S. Haldane, "The causes of periodic or Cheyne-Stokes breathing," J. Physiol., vol. 38, pp. 401-419, 1909.
 36. S. Lahiri, K. H. Maret, M. G. Sherpa, and R. M. Peters, "Sleep and Periodic Breathing at High Altitude: Sherpa Natives Versus Sojourners," in High altitude and Man. ed. J. B. West, pp. 73-90, 1983.
 37. T. B. Waggener, P. J. Brusil, R. E. Kronauer, R. A. Gabel, and G. F. Inbar, "Strength and cycle time of high-altitude ventilatory patterns in unacclimatized humans," J. Appl. Physiol., vol. 56, pp. 576-581, 1984.
 38. B. Gothe, G. S. Longobardo, P. Mantey, M. D. Goldman, and N. S. Cherniack, Effects of Increased Inspired Oxygen and Carbon Dioxide on Periodic Breathing During Sleep.
 39. N. S. Cherniack and G. S. Longobardo, "Cheyne-Stokes Breathing: An Instability in Physiologic Control," New England Journal of Medicine, pp. 952-957, May 3, 1973.

40. S. M. Tenney and L. C. Ou, "Ventilatory Response of Decorticate and Decerebrate Cats to Hypoxia and CO₂," Respiration Physiology, vol. 29, pp. 81-92, 1977.
41. S. M. Tenney and L. C. Ou, "Hypoxic Ventilatory Response of Cats at High Altitude: An Interpretation of 'Blunting'," Respiration Physiology, vol. 30, pp. 185-199, 1977.
42. L. C. Ou, M. J. Miller, and S. M. Tenney, "Hypoxia and Carbon Dioxide as Separate and Interactive Depressants of Ventilation," Respiration Physiology, vol. 28, pp. 347-358, 1976.
43. P. J. Lambertsen, P. Hall, H. Wollman, and M. W. Goodman, "Quantitative Interactions of Increased PO₂ and PCO₂ Upon Respiration in Man," Annals New York Academy of Sciences, pp. 731-741.
44. B. B. Lloyd, M. G. M. Jukes, and D. J. C. Cunningham, "The relation between alveolar oxygen partial pressure and the respiratory response to carbon dioxide in man," Q. J. exp. Physiol., vol. 43, pp. 214-227, 1958.
45. michel and milledge.
46. N. H. Edelman, P. E. Epstein, S. Lahiri, and N. S. Cherniack, "Ventilatory responses to Transient Hypoxia and Hypercapnia in Man," Respiration Physiology, vol. 17, pp. 302-314, 1973.
47. N. S. Cherniack, G. S. Longobardo, R. Levine, R. Mellins, and A. P. Fishman, "Periodic Breathing in Dogs.," J. Appl. Physiol., vol. 21, pp. 1847-1854, 1966.

48. R. Gilbert, J. H. Auchincloss, Jr., J. Brodsky, and W. Boden, "Changes in tidal volume, frequency, and ventilation induced by their measurement," J. Appl. Physiol., vol. 33, pp. 252-254, 1972.
49. M. A. Cohn, H. Watson, R. Weisshaut, F. Stott, and M. A. Sackner, "A transducer for noninvasive monitoring of respiration," Int. Symposium on Ambulatory Monitoring, ed, F. Stott, pp. 119-128, Academic Press, London, 1978. n
50. J. D. Sackner, A. J. Nixon, N. Atkins, and M. A. Sackner, "Non-invasive measurement of ventilation during exercise using the respiratory inductive plethysmograph," Am. Rev. Respir. Dis., vol. 122, pp. 867-871, 1980.
51. E. Tabacknik, N. Muller, and B. Toye, "Measurement of ventilation in children using the respiratory inductive plethysmograph," J. Pediat., vol. 99, pp. 895-899, 1981.
52. H. Watson, "The Technology of Respiratory Inductive Plethysmography," in Third International Symposium on Ambulatory Monitoring, Clinical Research Center, Harrow, Middlesex, U.K., 1979.
53. E. J. M. Campbell and J. B. L. Howell, "The Determination of Mixed Venous and Arterial CO₂ Tension by Rebreathing Techniques," in pH and Blood gas Measurement, pp. 101-108, Little, Brown & Co., Boston, 1959.
54. D. M. Band, M. McClelland, D. L. Phillips, K. B. saunders, and C. B. Wolff, "Sensitivity of the Carotid Body to Within Breath Changes in Arterial PCO₂," J. Appl. Physiol., vol. 45, pp. 768-777, 1978.

55. D. M. Band and C. B. Wolff, "Respiratory Oscillations in Discharge Frequency of Chemoreceptor Afferents in sinus Nerve of Anesthetized Cats at Normal and Low Arterial Oxygen Tension.," J. Physiol., vol. 282, pp. 1-6, 1978.
56. D. M. Band, K. B. Saunders, and C. B. Wolff, "The relation between chemoreceptor discharge and respiratory fluctuation of arterial pH in the anaesthetized cat," J. Physiol., pp. 73P-74P, July 1971.
57. N. W. Goodman, B. S. Nail, and R. W. Torrance, "Oscillations in the Discharge of Single Carotid Chemoreceptor Fibers in the Cat.," Resp. Physiol., vol. 20, pp. 251-269, 1978.
58. N. S. Cherniack and G. S. Longobardo, "Oxygen and Carbon Dioxide Gas Stores of the Body," Physiological Reviews, vol. 50, pp. 196-243, 1970.
59. F. S. Grodins, J. S. Gray, K. Schroeder, A. I. Norins, and R. W. Jones, "Respiratory Responses to CO₂ Inhalation; A Theoretical Study of a Nonlinear Biological Regulator.," J. Appl. Physiol., vol. 7, pp. 283-306, 1954.
60. R. K. Otnes and L. Enochson, Digital Time Series Analysis, John Wiley & Sons, New York, 1972.
61. R. O. Kenet, "Closed Loop Identification of Cardiovascular Control Systems," in PhD. Thesis, Yale University New Haven, Conn., May, 1983..
62. D. H. Kelly and D. C. Shannon, "Periodic breathing in infants with near-miss sudden infant death syndrome," Pediatrics, vol. 63, pp.

355-360, 1979.

63. D. Gordon, R. J. Cohen, D. H. Kelly, S. Akselrod, and D. C. Shannon, "Sudden Infant Death Syndrome: Abnormalities in Short Term Fluctuations in Heart Rate and Respiratory Activity," Pediatric Research, vol. In Press.
64. N. S. Cherniack, C. von Euler, I. Homma, and F. F. Kao, "Experimentally Induced Cheyne-Stokes Breathing.," Resp. Physiol., vol. 37, pp. 185-200, 1979.
65. R. L. Lange and H. H. Hecht, "The Mechanism of Cheyne-Stokes Respiration.," J. Clin. Invest., vol. 41, pp. 42-52, 1962.